

# *Early Tertiary transtension-related deformation and magmatism along the Tintina fault system, Alaska*

**Alison B. Till**

*U.S. Geological Survey, 4200 University Drive, Anchorage, Alaska 99508, USA*

**Sarah M. Roeske**

*Department of Geology, One Shields Avenue, University of California, Davis, California 95616-8605, USA*

**Dwight C. Bradley**

*U.S. Geological Survey, 4200 University Drive, Anchorage, Alaska 99508, USA*

**Richard Friedman**

*Department of Geological Sciences, University of British Columbia, Vancouver, British Columbia, Canada*

**Paul W. Layer**

*Department of Geological Sciences, University of Alaska, Fairbanks, Alaska 99704, USA*

## **ABSTRACT**

**Transtensional deformation was concentrated in a zone adjacent to the Tintina strike-slip fault system in Alaska during the early Tertiary. The deformation occurred along the Victoria Creek fault, the trace of the Tintina system that connects it with the Kaltag fault; together the Tintina and Kaltag fault systems girdle Alaska from east to west.**

**Over an area of ~25 by 70 km between the Victoria Creek and Tozitna faults, bimodal volcanics erupted; lacustrine and fluvial rocks were deposited; plutons were emplaced and deformed; and metamorphic rocks cooled, all at about the same time. Plutonic and volcanic rocks in this zone yield U-Pb zircon ages of ca. 60 Ma; <sup>40</sup>Ar/<sup>39</sup>Ar cooling ages from those plutons and adjacent metamorphic rocks are also ca. 60 Ma. Although early Tertiary magmatism occurred over a broad area in central Alaska, metamorphism and ductile deformation accompanied that magmatism in this one zone only.**

**Within the zone of deformation, pluton aureoles and metamorphic rocks display consistent NE-SW–stretching lineations parallel to the Victoria Creek fault, suggesting that deformation processes involved subhorizontal elongation of the package. The most deeply buried metamorphic rocks, kyanite-bearing metapelites, occur as lenses adjacent to the fault, which cuts the crust to the Moho (Beaudoin et al., 1997). Geochronologic data and field relationships suggest that the amount of early Tertiary exhumation was greatest adjacent to the Victoria Creek fault.**

**The early Tertiary crustal-scale events that may have operated to produce transtension in this area are (1) increased heat flux and related bimodal within-plate magmatism, (2) movement on a releasing stepover within the Tintina fault system or on a regional scale involving both the Tintina and the Kobuk fault systems, and (3) oroclinal bending of the Tintina-Kaltag fault system with counterclockwise rotation of western Alaska.**

**Keywords:** Tertiary, Tintina fault system, exhumation, crustal extension, transtension, tectonics, geochronology, metamorphism, oroclinal bending, Alaska.

## INTRODUCTION

The Tintina fault system is a major crustal-scale strike-slip system that stretches over 2000 km from southern British Columbia to western Alaska (Fig. 1). Despite its great length, the fault system's history remains largely enigmatic.

For much of its trace in Canada, the Tintina fault system parallels ancient facies boundaries and structural trends, making identification of piercing points and offset history challenging (Roddick, 1967). Estimates of total offset along the Tintina system have been as high as 1000 km (Gabrielse, 1985). Several workers using relations in Canada and in Alaska have estimated 450 km of offset (e.g., Tempelman-Kluit, 1979; Dover, 1994). Inception of movement on the fault system is thought to have occurred in the Paleozoic (Gabrielse, 1985) or mid-Cretaceous (Tempelman-Kluit, 1979) or Tertiary (Jackson and Mortensen, 2000). Local nonmarine sedimentary basins that are distributed along the fault contain Late Cretaceous and Tertiary flora, suggesting to some that the fault was active during this time (Cushing et al., 1986; Dover, 1994). Apatite fission track ages of fault slivers in a restraining bend along the Alaska section of the fault indicate pulses of movement occurred at several different times during the Tertiary (Till et al., 2004). Recent activity has been recognized in central Alaska (Weber and Foster, 1982; Barker, 1986) and in Canada (Mortensen and Von Gaza, 1992).

In Alaska, the Tintina fault system can be readily mapped from the Canadian border into central Alaska along the southern boundary of the Yukon Flats basin (Fig. 2). In the southwestern corner of the basin, several fault splays curve southwestward. One of these connects with the Kaltag fault system (Dover, 1994, and references therein), which has a clear topographic expression from central Alaska westward to the Bering Sea. Like the Tintina system, the timing and magnitude of offset on the Kaltag can only be approximated, but significant slip must postdate a regional Early Cretaceous (112–110 Ma) intrusive event (Patton et al., 1994).

In central Alaska, an unusual exposure of metamorphic rocks along the Tintina fault system provides evidence that the system was active in the early Tertiary and was responsible for exhumation of midcrustal rocks. There, two regionally extensive metamorphic terranes, the Ruby and Yukon-Tanana terranes, flank the fault system. These two terranes underlie most of the Ruby geanticline and the Yukon-Tanana Upland (Fig. 2). A major exhumation event affected these terranes during the Early Cretaceous, based on  $^{40}\text{Ar}/^{39}\text{Ar}$  ages and contribution of the metamorphic rocks to sedimentary basins (Fig. 2; Patton et al., 1994; Dover, 1994; Roeske et al., 1995; Hansen and Dusel-Bacon, 1998; Dusel-Bacon et al., 2002). In contrast, the only known metamorphic rocks in central Alaska with early Tertiary cooling ages occur along the Victoria Creek fault, the splay of the Tintina system that connects with the Kaltag fault (Fig. 2). There, lenses of kyanite-bearing rocks with early Tertiary cooling ages sit immediately

adjacent to the fault trace. The lenses are associated with plutonic, bimodal volcanic, and sedimentary rocks of similar early Tertiary ages (Riefenstahl et al., 1997a).

This paper presents evidence that an early Tertiary metamorphic, deformation, and igneous event was focused between two strands of the Tintina fault system, the Tozitna and the Victoria Creek faults. Of particular interest is the relationship of thin, elongate slivers of kyanite-bearing rocks to the adjacent Victoria Creek strike-slip fault. Our work, which is reconnaissance in style, evaluates the metamorphic history of the elongate slivers and the tectonic processes that might have focused a large amount of exhumation along this strand of the Tintina fault system.

The Victoria Creek fault is a subvertical structure that has been imaged by seismic reflection and refraction experiments and cuts the entire thickness of continental crust (Beaudoin et al., 1994). The early Tertiary metamorphic rocks currently lie immediately northwest of the fault in a restraining bend of the greater Tintina-Kaltag fault system. This position is consistent with exhumation by contractional or transpressional processes. However, there is evidence for repeated pulses of uplift in the area of the restraining bend since the early Tertiary (Till et al., 2004) and for basin formation across a broad area in latest Cretaceous–early Tertiary time (Farmer et al., 2003; Till et al., 2005; Phillips and Saltus, 2005). The present geometry of the fault system likely does not represent its geometry during the early Tertiary.

We examine several hypotheses for producing exhumation of metamorphic rocks along a strike-slip fault system, including extension due to a dilational step-over during movement on the Tintina fault system on two different scales or related to development of the Alaska oroclinal.

## THE RAMPART BLOCK

In central Alaska, early Tertiary volcanic and plutonic rocks are widespread and cross boundaries between major crustal units (Fig. 2). Paleocene sedimentary rocks are known along the Tintina and Kaltag fault systems and in scattered small exposures flanking regional basins, such as the Yukon Flats basin (Fig. 2). However, it is notable that in only one area early Tertiary metamorphic rocks are exposed in close proximity to early Tertiary volcanic, plutonic, and sedimentary rocks. There, plutonic rocks show evidence of deformation accompanying their emplacement. Early Tertiary plutons outside the area do not show signs of deformation. The early Tertiary metamorphic rocks and syntectonic plutons occur between two splays of the Tintina fault system, the Tozitna and Victoria Creek faults (Fig. 2). We refer to this region as the Rampart block (Fig. 2).

Pre-Tertiary bedrock units within the Rampart block have a close affinity to major units north of the block exposed in the Ruby Geanticline and Brooks Range; their affinity to rocks south of the Victoria Creek fault is limited. Within the Rampart block,

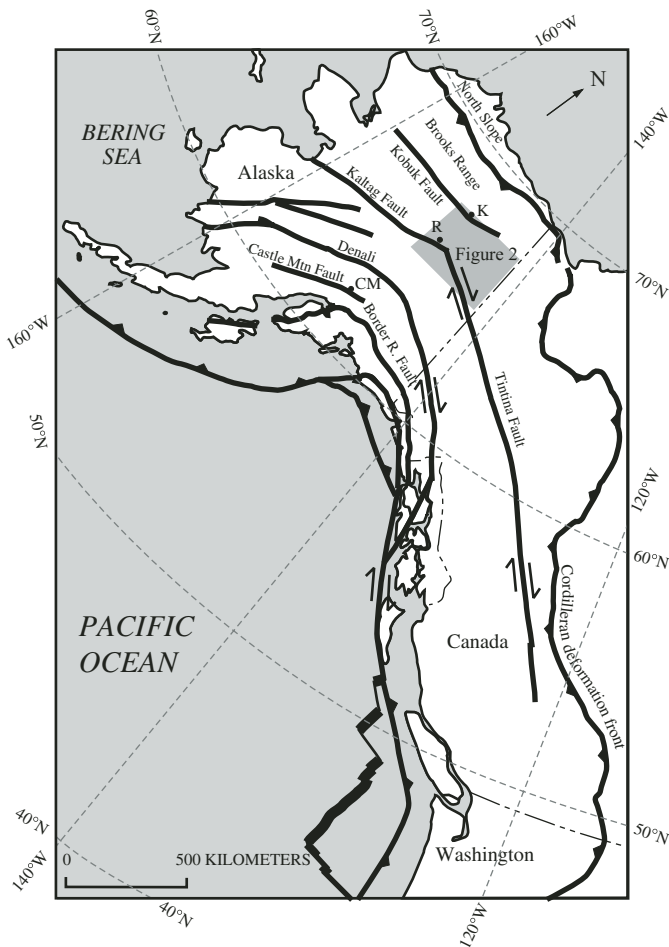


Figure 1. The northwestern North American continent showing location of major fault systems and early Tertiary metamorphic complexes discussed in the text. R = Rampart block, including the Minook and Raven Creek Hill complexes. K = amphibolite-facies rocks exhumed along the Kobuk fault zone. CM = greenschist-facies rocks exhumed along the Castle Mountain fault zone.

major pre-Tertiary bedrock units are the Tozitna terrane of oceanic affinity and the Devonian metaclastic sequence (Figs. 2, 3). The Tozitna terrane is an assemblage of Devonian to Jurassic chert, basalt, gabbro, and fine-grained clastic rocks characterized by brittle deformation fabrics and generally very low to low metamorphic grade (Patton et al., 1994; Dusel-Bacon et al., 1989). Tozitna terrane rocks in the Rampart block yielded K-Ar ages as old as Triassic (Brosgé et al., 1969) and lack signs of any significant deformation and metamorphism. The Devonian metaclastic sequence, originally described by Dover (1994), is composed of low-grade metasedimentary rocks, predominantly shale and slate, with subordinate metasandstones, carbonate rocks, and mafic volcanic rocks. Both packages of rocks are thought to have reached low metamorphic grades by the Early Cretaceous (Dusel-Bacon et al., 1989). The Devonian metaclastic sequence is interpreted to sit structurally below the Tozitna terrane across much of the Rampart block. The protolith packages of the

Devonian metaclastic sequence and the metamorphic rocks exposed along the SE boundary of the Rampart block are likely related. Metaquartzites from the units contain very similar detrital zircon populations that are dominated by Mesoproterozoic and older ages (Bradley et al., 2004).

South of the Victoria Creek fault, major pre-Tertiary bedrock units include several sequences of Proterozoic(?) and Paleozoic rocks, a Mesozoic marine sedimentary sequence, and the Yukon Tanana Upland, which is underlain by a vast assemblage of metamorphic and igneous rocks that extends more than 600 km to the SE. Close correlations cannot be made between rocks of any unit older than early Tertiary on either side of the fault, with one minor caveat. There are Proterozoic(?) and Paleozoic metasedimentary rocks on the north side of the Victoria Creek fault northeast of the study area (Fig. 3). Combined gravity and aeromagnetic data indicate that those rocks are a thin slab underlain by rocks with a geophysical character identical to the Tozitna terrane (Saltus et al., 2004), and they are shown as a thrust slice NW of the Victoria Creek fault (Fig. 3). The slab of metasedimentary rocks could have been overthrust as recently as the Tertiary, in light of apatite fission track ages from the Rampart block (Till et al., 2004). Thus, the southern boundary of the Rampart block, the Victoria Creek fault, marks a significant discontinuity in the nature of pre-Tertiary bedrock in central Alaska.

The western and eastern extent of the Rampart block cannot be precisely located based on existing geologic mapping and geochronology; the full regional extent of the early Tertiary deformational event is not known.

### Early Tertiary Rocks of the Rampart Block

Metamorphic rocks with early Tertiary cooling ages have been identified in five places in the Rampart block (four are shown on Fig. 3). The highest pressure and most extensive metamorphic rocks are exposed in two elongate lenses adjacent to the Victoria Creek fault. In the northeastern of the two lenses, Raven Creek Hill, a white mica-bearing alaskite pluton is intimately associated with kyanite-grade metapelite. In the better exposed and more extensive southwestern lens, the Minook complex, metasedimentary and minor metaigneous lithologies are cut by basaltic and felsic dikes, and early Tertiary basalt and rhyolite occur nearby. About 35 km NW of the Minook complex, early Tertiary metamorphic rocks at Senatis Mountain and Vertical angle elevation bench mark (VABM) Shale contain mineral assemblages consistent with lower pressure peak metamorphic conditions than those found at the Minook complex or Raven Creek Hill. The fifth occurrence of metamorphic rocks is associated with the Yukon Rapids granite, a large elongate early Tertiary pluton. Intense flattening and stretching is manifested in ductile fabrics in its contact aureole; the pluton itself locally contains a tectonic fabric.

Early Tertiary volcanic rocks in the Rampart block include both rhyolite and basalt with within-plate chemical signatures (Fig. 4; Riefenstahl et al., 1997a). Bimodal dikes cut both the Minook complex metamorphic rocks and the Devonian-Jurassic

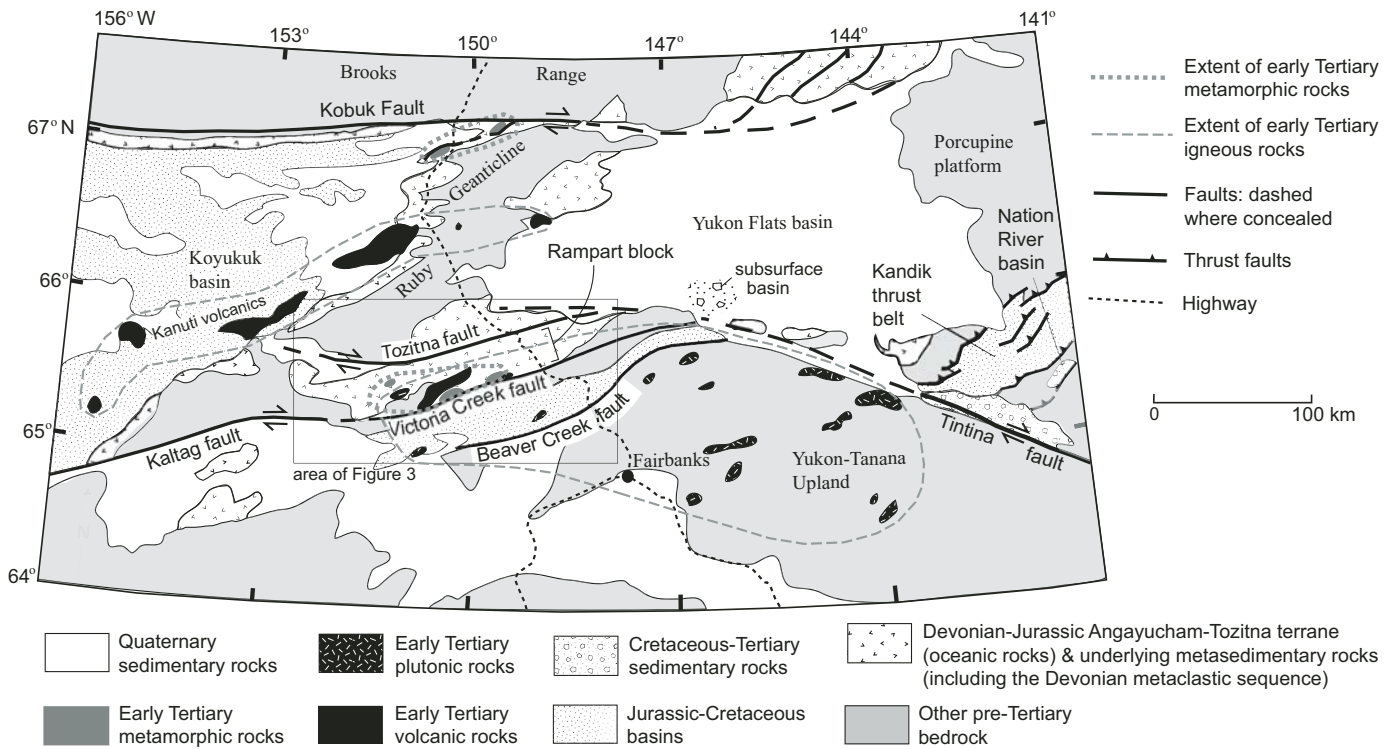


Figure 2. Major crustal features and early Tertiary rock units along the Tintina fault system in central Alaska.

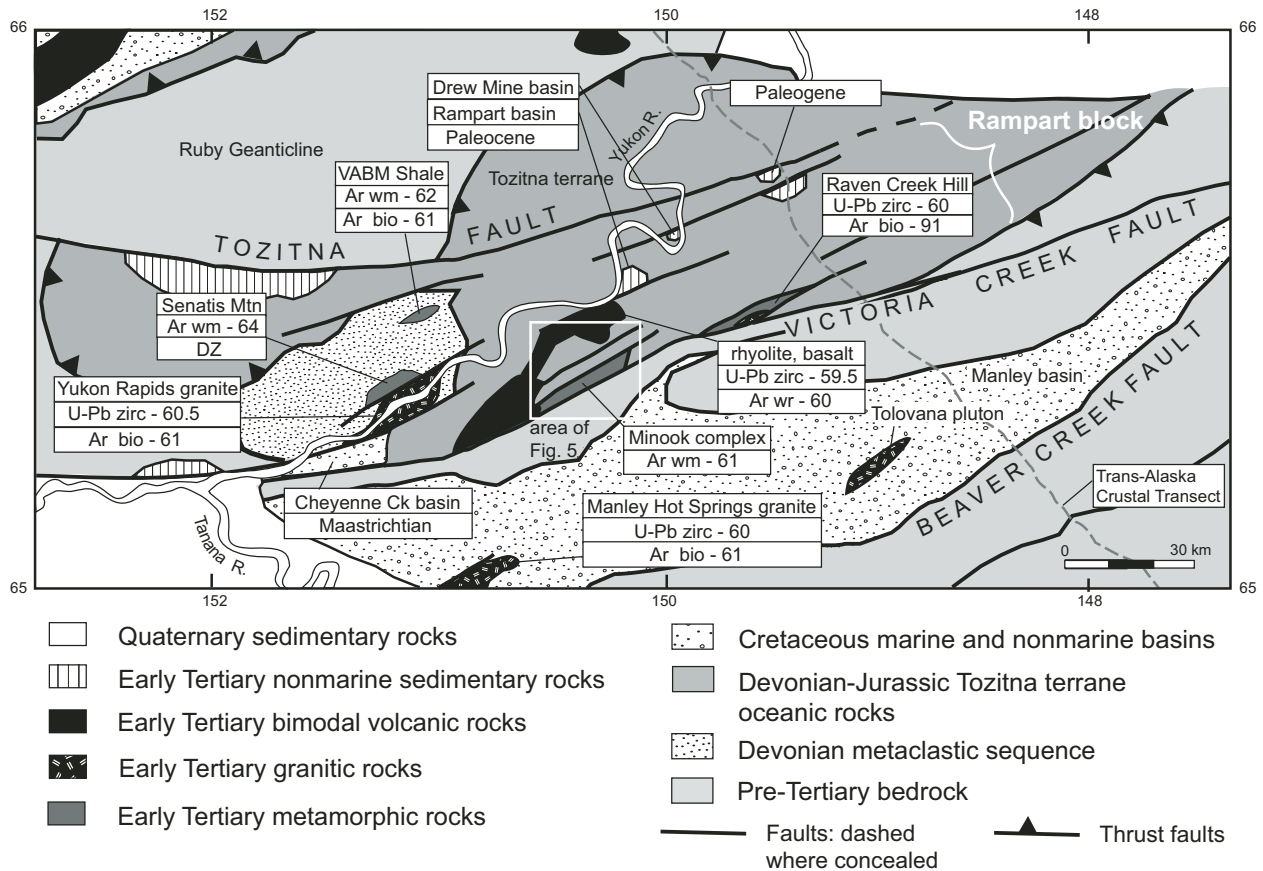


Figure 3. Geologic map and geochronology sample locations, Rampart block and adjacent area. Ar— $^{40}\text{Ar}/^{39}\text{Ar}$  age; U-Pb—zircon crystallization age; DZ—detrital zircon sample location. Wr—whole rock; wm—white mica; zirc—zircon.

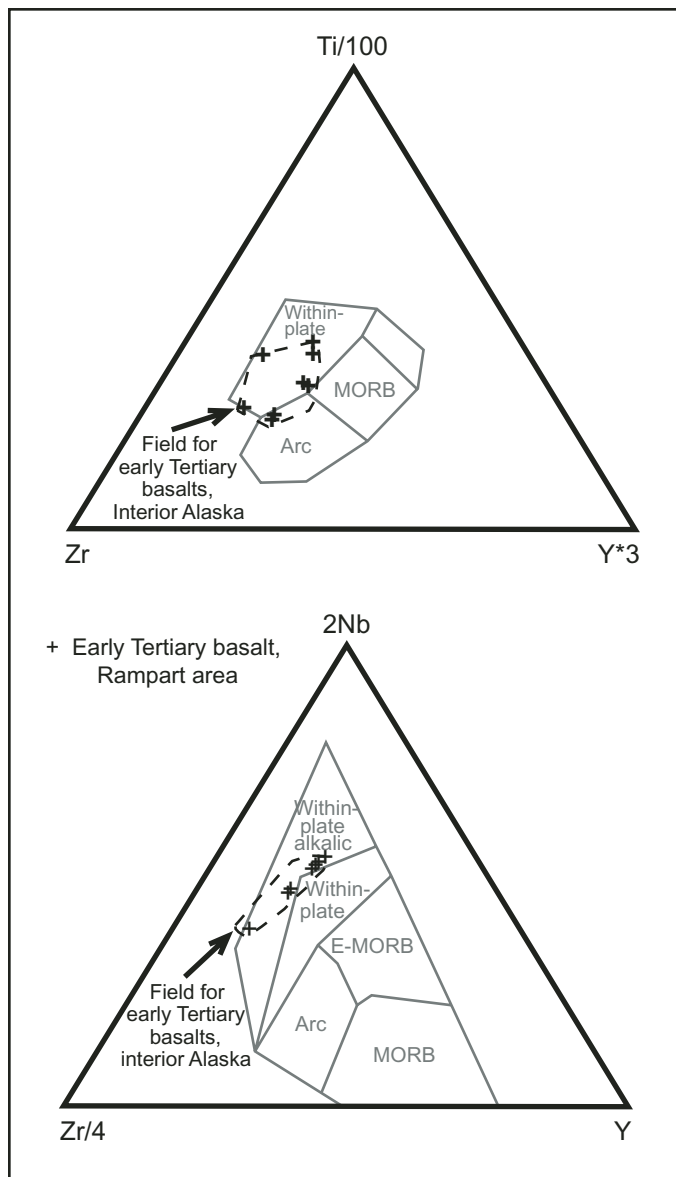


Figure 4. Trace element discriminant plots for early Tertiary basalts from the Rampart area and interior Alaska, from Newberry and Haug (1997) and Newberry (2000).

Tozitna oceanic rocks, indicating that all were in proximity during the early Tertiary magmatic episode. The volcanics were erupted onto a paleosurface dominated by the Tozitna terrane, which underlies much of the Rampart block (Riefenstuhl et al., 1997a).

Exposures of latest Cretaceous and early Tertiary sedimentary rocks in the Rampart block are widely scattered (Farmer et al., 2003). The oldest, the Cheyenne Creek basin, is Maastrichtian and sits in fault contact with the younger Yukon Rapids granite (Fig. 3). Paleocene palynomorphs have been identified in the Rampart and Drew Mine sedimentary sections. Clast compositions indicate that the sediments in these two Paleocene sections were derived from the Tozitna terrane; the sections contain coal

and lacustrine facies. Facies, paleocurrents, and clast compositions of the Paleocene sections differ from those in the Maastrichtian sequence, indicating a change in tectonic influences on deposition at the Maastrichtian/Paleocene boundary (Farmer, 2004).

An early Tertiary crustal section can be reconstructed using the relationships described above. Bimodal volcanic rocks sat in depositional contact with the Tozitna terrane, as did Paleocene lacustrine and fluvial sedimentary rocks, which contain detritus derived from the Tozitna (Farmer et al., 2003). The metamorphic rocks of the Minook complex cooled through the closure temperature of argon in mica around 60 Ma and, therefore, sat at some depth in the crust while the volcanic and sedimentary rocks were deposited on the Tozitna terrane. In present exposures, the part of the early Tertiary crustal section that sat between the Tozitna terrane and the hot metamorphic rocks is apparently missing. The crustal depth of the metamorphic rocks in the early Tertiary is the crucial factor in determining how much crust was excised from the section during exhumation of the metamorphic rocks.

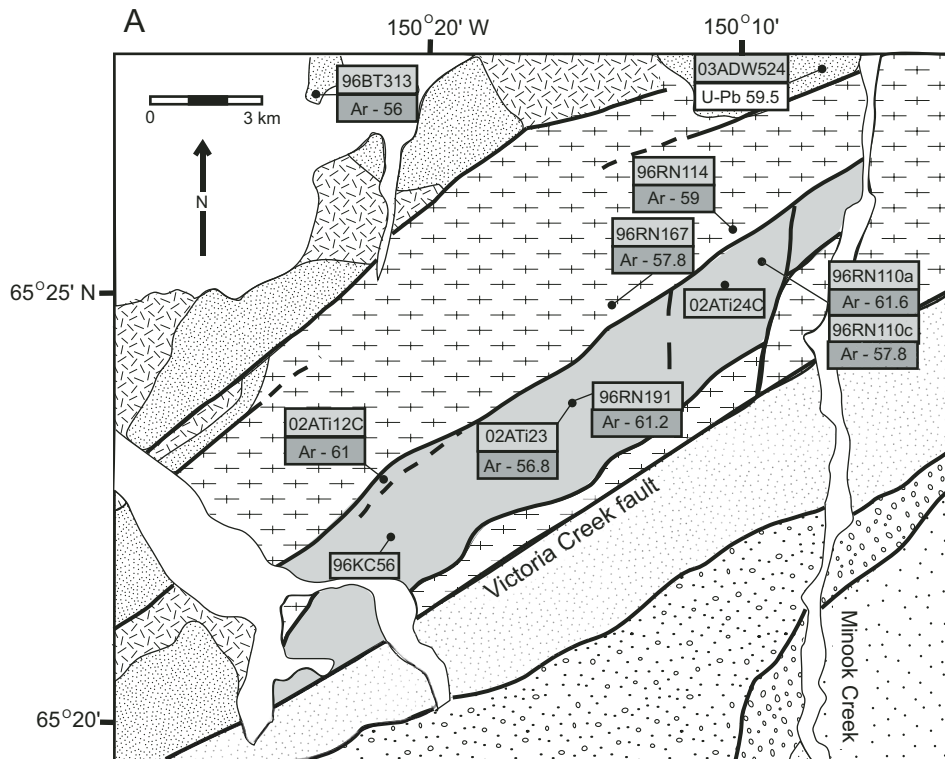
The juxtaposition of early Tertiary bimodal volcanics and the Tozitna terrane with metamorphic rocks that have early Tertiary cooling ages suggests extensional faults may have been responsible for exhumation of the metamorphic rocks along the Victoria Creek fault. Because apatite fission-track evidence shows that the faults that separate the metamorphic rocks from the adjacent Tozitna terrane and volcanic rocks are younger than early Tertiary (Till et al., 2004), any extensional faults active during the early Tertiary have been overprinted, reactivated, and rotated. The geometry of early Tertiary structures is therefore obscure. However, we may be able to infer the nature of early Tertiary events in the Rampart block. We will show below why we think a significant amount of crust was excised adjacent to the Victoria Creek fault in early Tertiary time.

## METAMORPHIC ROCKS OF THE RAMPART BLOCK

### Metamorphic Rocks near the Victoria Creek Fault

Metamorphic rocks of the Minook complex and Raven Creek Hill occur as elongate lenses adjacent to the Victoria Creek fault. The two lenses are 20 km apart.

The lens of schists exposed at the Minook complex underlies a single ridge and is ~17 km long by 1.5–2 km wide. Exposure is intermittent along the tundra-covered ridgeline and rare on its tree-covered flanks (Riefenstuhl et al., 1997a). The metamorphic section is composed of medium- to coarse-grained metapelitic and metaquartzitic schist, marble, calcareous schist, amphibolite, and one section of quartz-pebble metaconglomerate. Metapelite and metaquartzite are the most common lithologies. Along the northwest side of the complex, a sliver of finer-grained, graphitic metapelite less than 400 m wide sits between the schists and the widely exposed, very low-grade mafic rocks of the Tozitna terrane (Fig. 5). The contact between the graphitic metapelites and the Tozitna terrane appears to be a vertical fault; the geometry of the contact of



### North of Victoria Ck fault

- Tertiary rhyolite
- Tertiary basalt
- Tertiary metamorphic rocks
- Devonian to Jurassic Tozitna terrane
- 30° strike and dip of foliation

### South of Victoria Ck fault

- Jurassic to Cretaceous sandstone and shale
- Permian to Triassic sandstone, shale, limestone
- Proterozoic (?) and Paleozoic chert, volcanic rocks, limestone, dolostone
- Proterozoic (?) and Paleozoic sandstone ("grit"), argillite

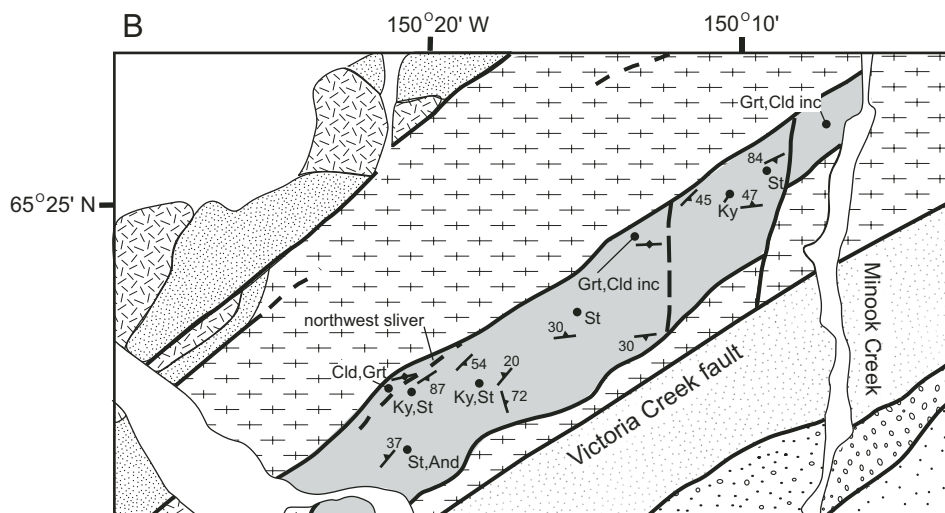


Figure 5. Geologic map, sample locations, and selected metamorphic and structural data, Minook complex. A—sample locations and argon ages; B—structural data and key mineral localities. Ar— $^{40}\text{Ar}/^{39}\text{Ar}$  age; U-Pb—zircon crystallization age. St—staurolite; ky—kyanite; and—andalusite; grt—garnet; cld inc—chloritoid inclusion.

the graphitic metapelites and the schists is difficult to discern. On the southeast side, Tozitna terrane metagabbros sit above the complex on a south-dipping brittle fault (Riefenstahl et al., 1997a).

Within the small metamorphic complex, rock fabrics and mineral textures vary considerably, although most mineral parageneses generally reflect similar peak metamorphic conditions (Table 1). Staurolite, garnet, biotite, and kyanite are common within the main schist package. Foliation in pelitic rocks varies from intensely planar to weakly developed (Fig. 6). Lineations are defined by elongate kyanite and garnet or trains of micas or staurolite and garnet. More quartz-rich rocks display the most even, planar fabrics and

the best-developed mineral lineations. Schists that contain the assemblage biotite-garnet-staurolite retain relict primary lithologic layering (96RN128, Fig. 6A), or have classic coarse-grained porphyroblastic textures with large, round to elongate garnets and idioblastic micas (96RN163, Fig. 6B). Kyanite-bearing rocks include those that have idioblastic textures and weakly formed fabrics (not pictured) and those that have strong fabrics defined by concentrations of strongly parallel, lensoid micas, and needle-shaped to elongate porphyroblasts (02ATi24C; Figures 6G, 6H).

Kyanite growth accompanied deformation. Elongate kyanite lies in the foliation with biotite and white mica in samples

TABLE 1. REPRESENTATIVE METAPELITIC ASSEMBLAGES, RAMPART AREA, CENTRAL ALASKA

Area	Sample number	bt	grt	st	ky	crd	and	cld	chl	cal	ilm	hem	opaq	gr	tur	other
<u>Minook complex</u>																
NW	02ATi12*	x	x			x							x	x		
	02ATi13	x	x			x							x	x		
Main	02ATi32A	x	x					x†		x			x			
	02RSR18a	x	x					x†					x			
	02RSR26d	x	x									x	x		x	
	02ATi14B	x		x	x								x	x		pl
	96RN128	x	x	x									x		x	pl
	96RN110a*	x	x	x											x	
	96RN163	x	x	x									x	x		
	02ATi19A			x	x				x				x	x	x	
	02ATi24C	x	x	x†	x										x	
	SW	96KC56	x	x	x			x				x	x			
<u>Raven Creek Hill</u>																
	02ATi27C	x		x	x				x							
	02ATi27D	x		x					x				x	x		pl
	02ATi27E	x	x	x									x			pl
	02ATi27G*	x			x				x							rt
<u>VABM Shale</u>																
	85Ado75*	x					x						x	x	x	
	85Ado76*	x											x	x		pl
<u>Senatis Mountain</u>																
	02RSR13b*	x													x	rt, zrn
	02ATi22E	x	x				x					x	x			45% and
	02ATi22C	x	x				x	x†				x	x		x	no white mica
<u>Manley pluton contact aureole</u>																
	03ATi46B	x	x			x	x									
<u>Yukon Rapids pluton contact aureole</u>																
	02ATi20	x				x					x		x			gedrite, rare qtz, no white mica

Note: All mineral assemblages contain quartz and muscovite unless noted in "other" column. Abbreviations after Kretz (1983): and—andalusite, bt—biotite, cal—calcite, chl—chlorite, cld—chloritoid, crd—cordierite, grt—garnet, gr—graphite, hem—hematite, ilm—ilmenite, ky—kyanite, pl—plagioclase, qtz—quartz, rt—rutile, st—staurolite, tur—tourmaline, zrn—zircon; opa—opaque.

\*Analyzed for  $^{40}\text{Ar}/^{39}\text{Ar}$ .

†Occurs as inclusion in garnet.

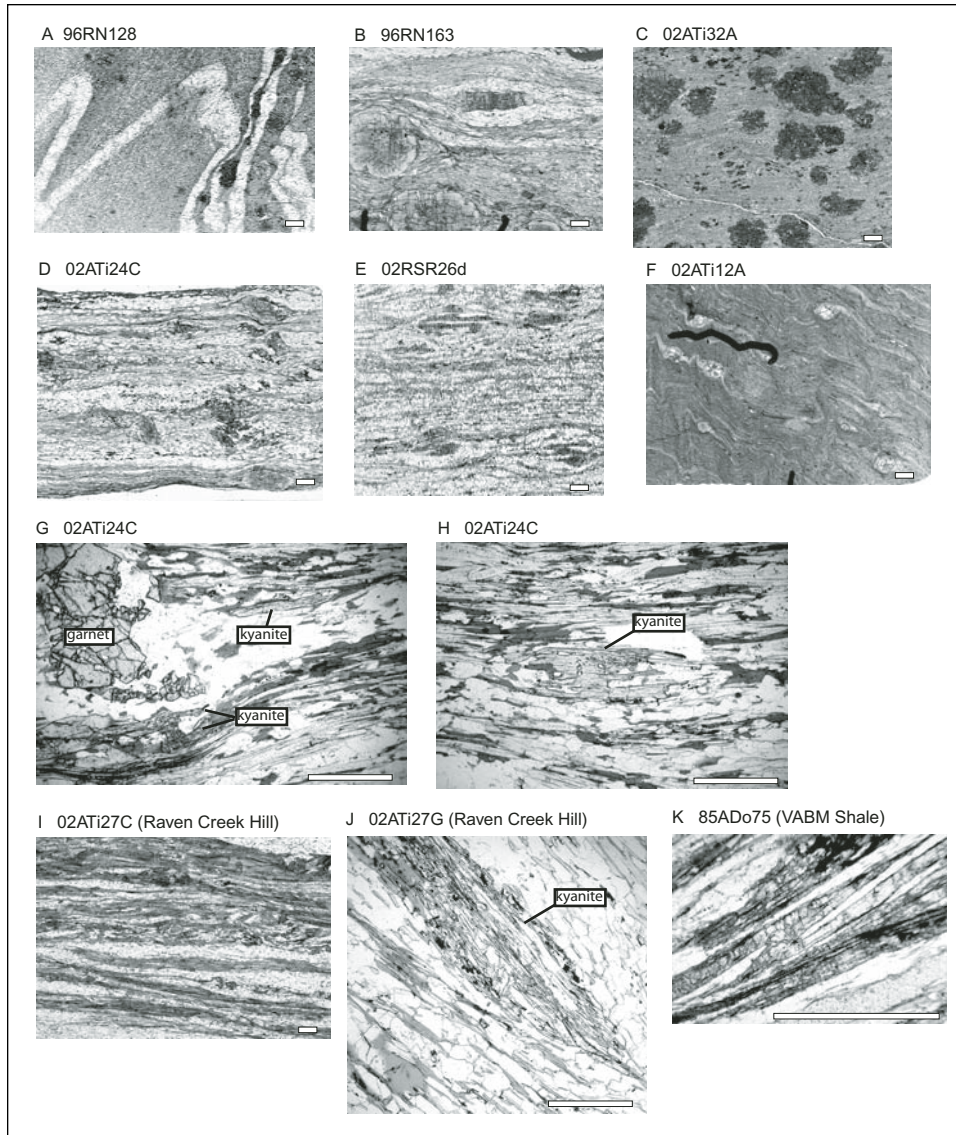


Figure 6. Images of representative rock fabrics, Minook and Raven Creek Hill. Images A–F and I are digital scans of partial thin sections, approximately one quarter of the section; images G, H, J, and K are photomicrographs. Bar in lower right of each image is one millimeter long. Images are from the Minook complex unless otherwise noted. (A) Quartz-rich and pelitic layering is preserved in this weakly foliated sample; staurolite, garnet, and biotite are developed in the darker layers. (B) Garnet porphyroblast shapes vary from round to oblate to strongly oblate in this garnet-staurolite-biotite rock. (C) Poikiloblastic garnets in weakly foliated biotite-garnet metapelite. (D) Strongly foliated sample with stable assemblage of garnet-kyanite-biotite with staurolite inclusions in garnet. Equilibrated above the staurolite-out reaction. Garnet porphyroblasts vary in size and shape, some idioblastic, some irregular. Photomicrographs G and H are from this sample. (E) Strongly foliated garnet-staurolite-biotite sample showing lens-shaped garnet porphyroblasts. (F) Small idioblastic garnets and cordierite poikiloblasts in fine-grained schist. Cordierite poikiloblasts appear as slightly paler gray zones; one is below the hooked right-hand end of the black ink line. (G) Prism-shaped kyanite grains in sample 02ATi24C, aligned in foliation as it wraps around garnet porphyroblast. (H) Kyanite grain from sample 02ATi24C aligned in foliation. (I) Kyanite-staurolite-biotite schist with biotite aligned in elongate lenses. (J) Kyanite grain aligned in foliation of sample 02ATi27G. (K) Z-shaped andalusite grain aligned in foliation of sample 85ADo75 from VABM Shale, showing dynamic nature of early Tertiary low-pressure metamorphism at that locality.

from both the Minook complex and Raven Creek Hill (Figs. 6G, 6H, 6I, 6J). In some samples, kyanite grains are needle-shaped and were initially thought to be sillimanite. The parallelism of the elongate kyanite with lineation-defining porphyroblasts and micas, as well as the extremely elongate crystal shape of kyanite in several samples, are indications that kyanite growth accompanied the major period of ductile deformation.

Pelitic mineral assemblages present in the Minook complex are represented on an AFM ( $A = \text{Al}_2\text{O}_3 - 3\text{K}_2\text{O}$ ;  $F = \text{FeO}$ ;  $M = \text{MgO}$ ) diagram in Figure 7. The assemblages staurolite-garnet-biotite and garnet-biotite-kyanite are relatively common in these rocks (Fig. 7A). Garnets in one sample, 02ATi24C, contain staurolite inclusions, but the matrix of the rock lacks staurolite. The stable paragenesis is kyanite-biotite-garnet (Fig. 7B). This sample passed through the terminal staurolite-out reaction, a transition

that is represented as the difference between panels A and B on Figure 7. Taken together, and assuming no major faults between the samples, the assemblages present suggest that peak metamorphic conditions at the Minook complex were in the vicinity of the staurolite-out reaction in the kyanite field. Sample 02ATi24C may have a bulk composition that resulted in slightly lower temperature destabilization of staurolite than the other samples.

Garnets in staurolite-bearing assemblages show weak prograde zoning with no signs of retrograde reequilibration near the rims. Some samples contain two textural types of garnets: coarse, idioblastic to moth-eaten garnets and fine, idioblastic garnets. The rims of the coarser garnets have the same composition as the idioblastic garnets, which are very weakly zoned (Fig. 8).

Rocks collected along the northwest side of the Minook complex are very fine-grained schists with a single simple fab-

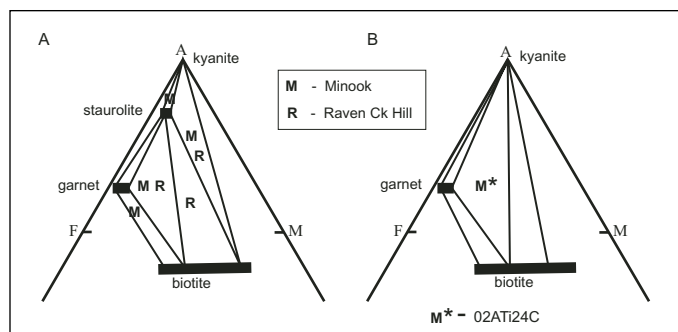


Figure 7. AFM plots for pelitic assemblages, Minook complex and Raven Creek Hill. Letters M and R represent assemblages documented at each area. (A) Staurolite zone assemblages, (B) kyanite zone assemblages above staurolite-out reaction.

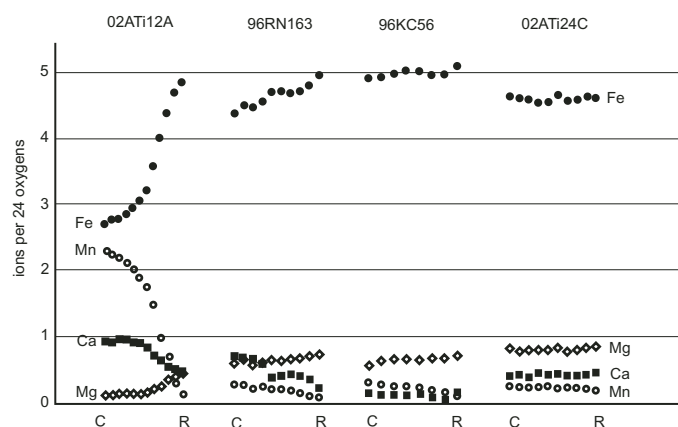


Figure 8. Microprobe analytical traverses of garnets from samples from the Minook complex. These traverses are representative of multiple detailed traverses on multiple garnets from each sample. Analyses acquired on the Cameca SX-100 electron microprobe, University of California, Davis.

ric and either poikiloblastic or small idioblastic porphyroblasts (02ATI32A, 02ATI12A; Figs. 6C, 6F). The poikiloblastic garnets in 02ATI32A contain chloritoid inclusions, though chloritoid is absent in the matrix. Garnet and biotite are the stable indicator minerals in 02ATI32. This assemblage is stable in metapelites at a range of conditions, including staurolite-zone conditions (Fig. 7).

Some of the fine-grained schists on the northwest side of the Minook complex contain mineral assemblages crystallized at distinctly different conditions than the rest of the Minook schists. The assemblage in sample 02ATI12A, garnet-cordierite-biotite, is stable at low pressures. Concentrations of white mica and quartz in mm-thick lenses and long, thin tails developed in the pressure shadows of the garnets accentuate the fine, laminar nature of the foliation. Elongate cordierite porphyroblasts and trains of biotite in some samples define a mineral lineation. Garnets are fine and idioblastic, and their compositional profiles show very strong zoning of iron and magnesium (Fig. 8). There is no indication that

this rock contained an earlier fabric or was recrystallized from rocks that once contained chloritoid, staurolite, or kyanite. We will refer to these metamorphically distinct rocks as “the northwest sliver.”

One sample from the main part of the Minook complex, 96KC56, contains a secondary assemblage that preserves evidence of an exhumation path. The assemblage staurolite-biotite-garnet records peak conditions reached by this sample. Locally staurolite was replaced by biotite and andalusite (Fig. 9). Staurolite porphyroblasts contain patches of andalusite with small inclusions of biotite and remnants of staurolite. Biotite overgrew rims and invaded cracks in the porphyroblast. Some grains of staurolite were completely replaced. Andalusite also grew in polycrystalline lenses where the foliation wraps around rims of garnet and staurolite. These relationships record a staurolite-out reaction at low pressures. This rock was collected near the SW end of the Minook complex (Fig. 5B). Except for those just described, textures in 96KC56 do not show evidence of the second crystallization event. The micas aligned in the foliation lack any sign of static recrystallization, and garnet lacks retrograde zoning (Fig. 8).

Raven Creek Hill is a rounded, tree- and tundra-covered ridgeline with rare rock outcrops. Based on reconnaissance mapping, metamorphic and plutonic rocks make up a lens ~9 km long and 1.5 km wide. The contact between the metapelitic schists and an alaskite pluton is exposed just off of the ridgeline on its southeast side. The pluton is also exposed 300 m below along the creek bottom. Near the contact and in the creek bottom, the alaskite pluton is texturally complex. It consists of medium-grained equigranular to seriate granite that appears to grade into a pegmatitic phase with no clear crosscutting relationship. In some

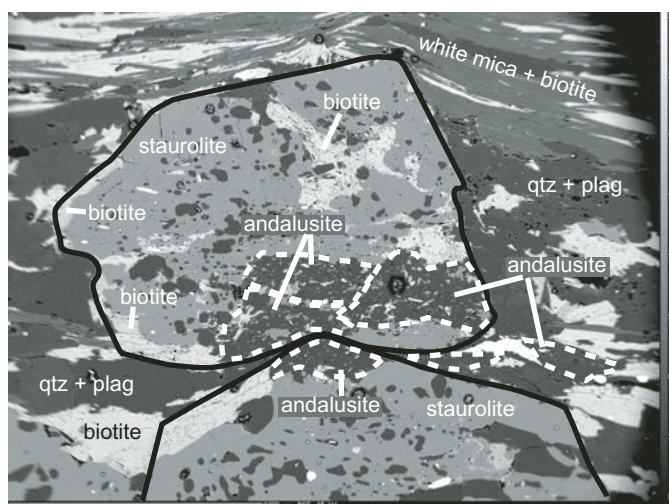


Figure 9. Electron backscatter image of pseudomorph after staurolite in sample 96KC56. Black outlines indicate original staurolite porphyroblasts; dashed white lines delineate andalusite grains; andalusite zones within the original staurolite porphyroblasts have optical continuity and inclusions of biotite and staurolite remnants; andalusite in the matrix occurs as masses of very fine grains. Image acquired on a Cameca SX-100 electron microprobe at 15 Kev, 40 namp.

outcrops near the contact, multiple thin (1–3 cm) pegmatite layers parallel one another and are rhythmically spaced 10–15 cm apart (Fig. 10). Very coarse grains are also scattered within the finer-grained material, and there is no identifiable sharp contact between the pegmatite and finer-grained phase. The alaskite contains accessory zircon, monazite, white mica, garnet, tourmaline, and dumortierite, an aluminoborosilicate. In thin section, some samples of the alaskite show no signs of strain and contain single populations of white mica. Other samples have strained feldspars with fine neoblasts concentrated on grain boundaries and two sizes of white mica, one coarse and one very fine; the very fine mica locally forms beards on the coarser one.

Typical metamorphic assemblages in the adjacent metapelitic rocks are listed in Table 1, and include biotite, garnet, staurolite, and kyanite. The metamorphic assemblages present at Raven Creek Hill are similar to those present at the Minook complex (Fig. 7); no sillimanite or andalusite has been identified in any of the samples.

Metamorphic fabrics are more consistent at Raven Creek Hill than they are at the Minook complex. Metasedimentary rocks are moderately to strongly foliated with fabrics defined by concentrations of strongly parallel, lensoid micas and elongate porphyroblasts. Mineral lineations in the metamorphic rocks are defined by trains of biotite and aligned needles and blades of kyanite (Figs. 6I, 6J). Mineral lineations in the contact zone of the alaskite pluton are defined by abundant aligned blades of blue green tourmaline.

Sample 96KC56 from the Minook complex is the only sample collected from either metamorphic lens that shows any indication of recrystallization during exhumation. New mica growth has not overprinted foliation-forming micas in other samples, even where the micas are bent or folded. Garnet rims show no evidence of resorption (Fig. 8). Foliation forming micas are commonly lens shaped and particularly strongly aligned in samples from Raven Creek Hill (Fig. 6I); these also lack any sign of mimetic or cross-fabric recrystallization. Except for 96KC56, there is no textural evidence for secondary recrystallization due to exhumation or a thermal pulse postdating peak metamorphism.



Figure 10. Outcrop of alaskite at Raven Creek Hill showing 1–3-cm-thick layers of pegmatitic material. Some very coarse feldspars are also present between the layers. Horizontal field of view ~20 cm.

### Metamorphic Rocks in the Northwest Part of the Rampart Block

The area northwest of the Yukon Rapids pluton is underlain by metasedimentary and minor metaigneous rocks of the Devonian metaclastic sequence, which experienced pre-Late Cretaceous greenschist-facies metamorphism recorded in assemblages in pelitic and mafic rocks (Dusel-Bacon et al., 1989). In two small areas, one near the northern boundary of the Devonian metaclastic sequence, the other near the Yukon Rapids pluton, higher-grade metamorphic assemblages are developed that overprint the greenschist-facies minerals. In the northern area, higher-grade rocks are exposed in a limited zone within one kilometer of VABM Shale. There, pelitic schists with millimeter-scale laminations of biotite, white mica, and quartz exhibit shear bands that locally cross foliation and foliation that is tightly folded. Andalusite grains lie in the foliation (Fig. 6K) and are elongate in a NNE direction. Twelve kilometers south of VABM Shale, on Senatis Mountain, metapelitic rocks contain biotite, garnet, and andalusite. Foliation intensity is variable, and intrafolial isoclinal folds and folds of the foliation are present. Andalusite grains are commonly poikiloblastic and cross foliation; biotite commonly has random orientations. The full extent of the early Tertiary metamorphism in this part of the Rampart block is not known.

Metamorphic rocks in the contact aureole of the early Tertiary Yukon Rapids pluton include metaquartzite, marble, metabasalt, and an iron-rich amphibolite. The metabasalts are hornblende-plagioclase amphibolites, and the iron-rich amphibolites contain gedrite + plagioclase + biotite + cordierite + ilmenite + Fe-Cu sulfide. Strongly foliated fabrics defined by oriented micas and L-tectonite fabrics of aligned amphiboles are developed in outcrops closest to the granite (Fig. 11). Locally, thin ductile shear zones with trains of mica on their surfaces cut the foliation. The amphibolites of both mafic and iron-rich compositions have strong mineral lineations that parallel mineral lineations in the pluton. In other lithologies, the occurrence of linear fabric elements is inconsistent, despite the appearance of high strain in some rocks. Metamorphic assemblages, specifically cordierite and gedrite (Fe-amphibole) in the iron-rich amphibolite, indicate relatively high temperatures and low pressures of crystallization.

### GEOCHRONOLOGY

U-Pb and Ar-Ar geochronologic analyses were focused on confirming the age of granitic, volcanic, and metamorphic units in the Rampart block. Most of these ages cluster tightly at 60 Ma. Placing age constraints on evolution of the metamorphic rocks is of particular importance for understanding the role the Victoria Creek fault has played in exhumation processes. Metamorphic rocks of the Minook complex record both higher pressure (kyanite-bearing) and secondary lower pressure (andalusite-bearing) conditions. If both assemblages were stable during the early Tertiary, the metamorphic rocks must have been exhumed rapidly from a relatively deep crustal setting. If the higher-pressure assemblages



Figure 11. Outcrop of shear zone in the contact aureole of the Yukon Rapids pluton. Dark layers are composed of calc-silicate minerals, lighter layers of quartz and feldspar. Pencil in upper left corner is 14 cm long.

are relict of a Cretaceous metamorphic event and moved to shallower crustal levels before the early Tertiary, exhumation processes were slower. Whether rapid or slow, the exhumation process apparently was most efficient immediately adjacent to the strike-slip fault system.

A summary of geochronologic data from metamorphic and igneous rocks in the Rampart block and adjacent areas is presented in Table 2. See Figures 3 and 5 for sample locations.

### U-Pb GEOCHRONOLOGY

Conventional U-Pb ID-TIMS (isotope dilution thermal ionization mass spectrometry) geochronology was done to determine the magmatic ages of selected granitic and felsic volcanic rocks of the Rampart block and associated rocks. This work was conducted at the Pacific Centre for Isotopic and Geochemical Research in the Department of Earth and Ocean Sciences, University of British Columbia. Three granitic and two felsic volcanic rock units sampled for this study yielded zircon, and monazite was also recovered from three of these. Results are plotted on standard concordia diagrams (Fig. 12) and listed in Table 3. Analytical techniques appear in the Appendix.

Multiple concordant and overlapping zircon and/or equivalent monazite results were achieved for all samples. Interpreted ages are based upon average  $^{206}\text{Pb}/^{238}\text{U}$  dates and monazite  $^{207}\text{Pb}/^{235}\text{U}$  dates and, for one rock unit, the Raven Hill Creek alaskite, a weighted average of monazite  $^{207}\text{Pb}/^{235}\text{U}$  dates. This intrusion is represented by two samples and has somewhat complicated systematics, discussed separately below. All other samples yielded straightforward results. Ages from rocks within or adjacent to the Rampart block lie within the narrow range of  $59.5 \pm 0.5$  Ma to  $60.9 \pm 1.0$  Ma, whereas a felsite from the Kanuti volcanics some 70 km northwest of the block is older, at  $62.4 \pm 0.3$  Ma.

Two of the samples (Figs. 12B and 12F; Yukon Rapids pluton and the Kanuti felsite) include slightly younger and non-

overlapping zircon results interpreted to reflect very minor Pb loss. In these cases interpreted ages are based on older clusters of concordant and overlapping data. Inclusion of all data for these change interpreted ages by  $<0.5$  Ma. Zircon results for one of the samples (Fig. 12E; Manley Hot Springs pluton) suggest the presence of inherited components and/or Pb loss. Due to these complexities the average of two overlapping monazite  $^{207}\text{Pb}/^{235}\text{U}$  dates is taken as the best age estimate. This partially overlaps in age with results for two concordant zircon fractions (Fig. 12E, labeled E, C); the slightly younger zircon results may reflect minor Pb loss. Reported precisions for all of these interpreted ages are derived from the total range of Pb/U errors for averaged Pb/U data.

The Raven Hill Creek alaskite was sampled for U-Pb dating at two localities. Sample 02ATi28F was collected at the contact of the alaskite with the surrounding metamorphic rocks and contained both the medium-grained to seriate and pegmatitic variants of the alaskite. Sample 02ADW518 was collected several hundred meters below from a creekside outcrop. Both the finer-grained and pegmatitic variants were present at that locality as well, but only the finer-grained variant was submitted for analysis. Both samples from the alaskite yielded abundant monazite and lesser metamict zircon (only the former mineral was dated in this study). In addition, only from sample 02ATi28F, a modest amount of high-quality, clear, pink zircon was recovered and analyzed. A plot of all data from both samples (Fig. 12C) shows a cluster of six monazite analyses with equivalent  $^{207}\text{Pb}/^{235}\text{U}$  dates of ca. 111 Ma, and an array of younger monazite results as young as ca. 70 Ma. In addition, clear zircon from sample 02ATi28F gave concordant results at ca. 60 Ma. The six equivalent and oldest monazite results are taken as the best record of the original magmatic age of the alaskite; a weighted average of these six  $^{207}\text{Pb}/^{235}\text{U}$  dates yields an interpreted age of  $111.3 \pm 0.3$  Ma. The array of younger monazite data likely records various degrees of Pb loss from the analyzed grains. The younger zircons with ages of ca. 60 Ma are interpreted as primary magmatic grains from pegmatitic material intimately intermixed and closely associated with sample 02ATi28F and not present in the finer-grained material analyzed from 02ADW518. The young zircon results are plotted at an expanded scale on Figure 12D. An interpreted age of  $60.1 \pm 0.8$  Ma is the average  $^{206}\text{Pb}/^{238}\text{U}$  age and composite error for concordant fractions B, I, and J. Slightly younger results for fraction H are taken to indicate minor Pb loss that affected these grains.

### $^{40}\text{Ar}/^{39}\text{Ar}$ Geochronology

$^{40}\text{Ar}/^{39}\text{Ar}$  analyses of white mica, biotite, and biotite-rich parts of whole-rock separates from metamorphic and igneous rocks were done by laser step heating methods at the Geophysical Institute, University of Alaska, Fairbanks. The detailed analyses are given in Table 4. Ages in the geochronology summary in

TABLE 2. SUMMARY OF GEOCHRONOLOGIC DATA, RAMPART AREA, CENTRAL ALASKA

Sample types	Sample number	U/Pb Age (Ma)	Ar/Ar Age* (Ma)	Material	Location	
					Latitude (°N)	Longitude (°W)
<b>Plutonic rocks</b>						
Raven Creek Hill alaskite	02ATi28f†	111.3 ± 0.3	—	Monazite	65° 30.6582'	149° 35.6382'
Raven Creek Hill alaskite	02ADw518†	111.3 ± 0.3	—	Monazite	65° 30.6594'	149° 35.6076'
Raven Creek Hill alaskite, pegmatitic variant	02ATi28f†	60.1 ± 0.8	—	Zircon	65° 31.2228'	149° 34.9278'
Raven Creek Hill alaskite	96RN244§	—	83.3 ± 0.4	White mica	65° 31.1166'	149° 35.28'
Yukon Rapids granite	96RN243a§	—	60.0 ± 0.2	Zircon, Biotite	65° 19.632'	150° 03.42'
Yukon Rapids granite	02ADw506a†	60.5 ± 0.2	60.0 ± 0.2	Zircon, Biotite	65° 19.9488'	151° 03.426'
Manley Hot Springs granite	02ADw521a†	60.9 ± 1.0	58.7 ± 0.2	Zircon, Biotite	65° 01.542'	150° 43.0998'
Manley Hot Springs granite	96RN16§	—	58.7 ± 0.2	Zircon, Biotite	65° 01.542'	150° 43.0998'
<b>Volcanic units/dikes</b>						
Rhyolite	02ADw524b†	59.5 ± 0.5	—	Zircon	65° 28.2654'	150° 06.7704'
Rhyolite	96BT313§#	—	55.8 ± 0.3	Whole rock	65° 27.6204'	150° 23.22'
Basalt	96BT298b§#	—	60.0 ± 0.2	Whole rock	65° 29.3664'	150° 00.0'
Mafic dike	96RN110c§#	—	57.8 ± 0.3	Whole rock	65° 25.494'	150° 09.36'
Mafic dike	96RN114c§#	—	59.1 ± 0.3	Whole rock	65° 25.8126'	150° 10.2'
Trachyte dike	96RN167§#	—	57.8 ± 0.2	Whole rock	65° 24.7806'	150° 14.22'
<b>Metamorphic units/veins</b>						
Minook complex pelitic schist	96RN110a§	—	61.5 ± 0.2	White mica	65° 25.494'	150° 09.36'
Minook complex micaceous quartzite	02ATi23	—	56.8 ± 0.8	White mica	65° 23.5368'	150° 15.7284'
Minook complex vein that cuts schists	96RN191§	—	61.2 ± 0.3	White mica	65° 23.5674'	150° 15.6'
Minook complex cordierite schist, NW	02ATi12†	—	61.1 ± 0.3	Whole rock-biotite	65° 22.5858'	150° 21.711'
Raven Creek Hill pelitic schist	02ATi27G	—	90.6 ± 2.0	Biotite	65° 31.3686'	149° 34.875'
VABM Shale pelitic schist	85ADo75†	—	61.9 ± 0.4	White mica	65° 29.271'	150° 59.901'
VABM Shale pelitic schist	85ADo75†	—	60.9 ± 0.3	Biotite	65° 29.271'	150° 59.901'
Senatis Mtn. micaceous quartzite	02RSR13b†	—	64.5 ± 0.5	White mica	65° 20.979'	151° 07.812'
<b>Volcanic flow, NW of the study area</b>						
Kanuti felsic volcanic	02ATi36†	62.4 ± 0.3	—	Zircon	65° 24.927'	150° 01.326'

Note: VABM—Vertical angle elevation bench mark.

\*Plateau ages; plateau = >50% <sup>39</sup>Ar released, mean square of weighted deviates ≤2.5.

†This study.

§Reifenstuhl et al. (1997b).

#See Reifenstuhl et al. (1997b) for analytical data.

Table 2 and on the age spectrum diagrams (Fig. 13) are quoted to the ± 1 sigma level and calculated using the constants of Steiger and Jaeger (1977). The “integrated age” is the age given by the total gas measured and is equivalent to a potassium-argon (K-Ar) age. The “plateau age” as used here represents three or more consecutive gas fractions consisting of at least 50% of the total gas release that are within two standard deviations of each other (mean square weighted deviation less than ~2.5).

Reifenstuhl et al. (1997b) first demonstrated the early Tertiary age for metamorphic and igneous rocks in the Rampart block using <sup>40</sup>Ar/<sup>39</sup>Ar analyses from the same lab with the same methodology we have used. We include select analyses of samples from their data set with ours (see Table 2, Summary of Geochronologic Data, to see which analyses discussed here come from that original data set).

Age spectra and plots of apparent Ca/K values are shown in Figure 13.

### Minook Complex

White mica from a coarse-grained staurolite-garnet schist yielded a plateau age of 61.5 ± 0.2 Ma (sample 96RN110a). This age is similar to the isochron age of 62.0 ± 0.4 Ma (Fig. 14). Biotite-rich portions of a whole-rock sample from a fine-grained cordierite-garnet schist yielded a plateau age of 61.1 ± 0.3 Ma (sample 02ATi12C). Sample 02ATi23, white mica from a micaceous metaquartzite, yielded a plateau age of 56.8 ± 0.8 Ma and an isochron age of 57.2 ± 5.3 Ma (Fig. 14). At the same locality, white mica from a gold-quartz vein that crosses the metamorphic fabric produced a plateau age of 61.2 ± 0.3 Ma (sample 96RN191).

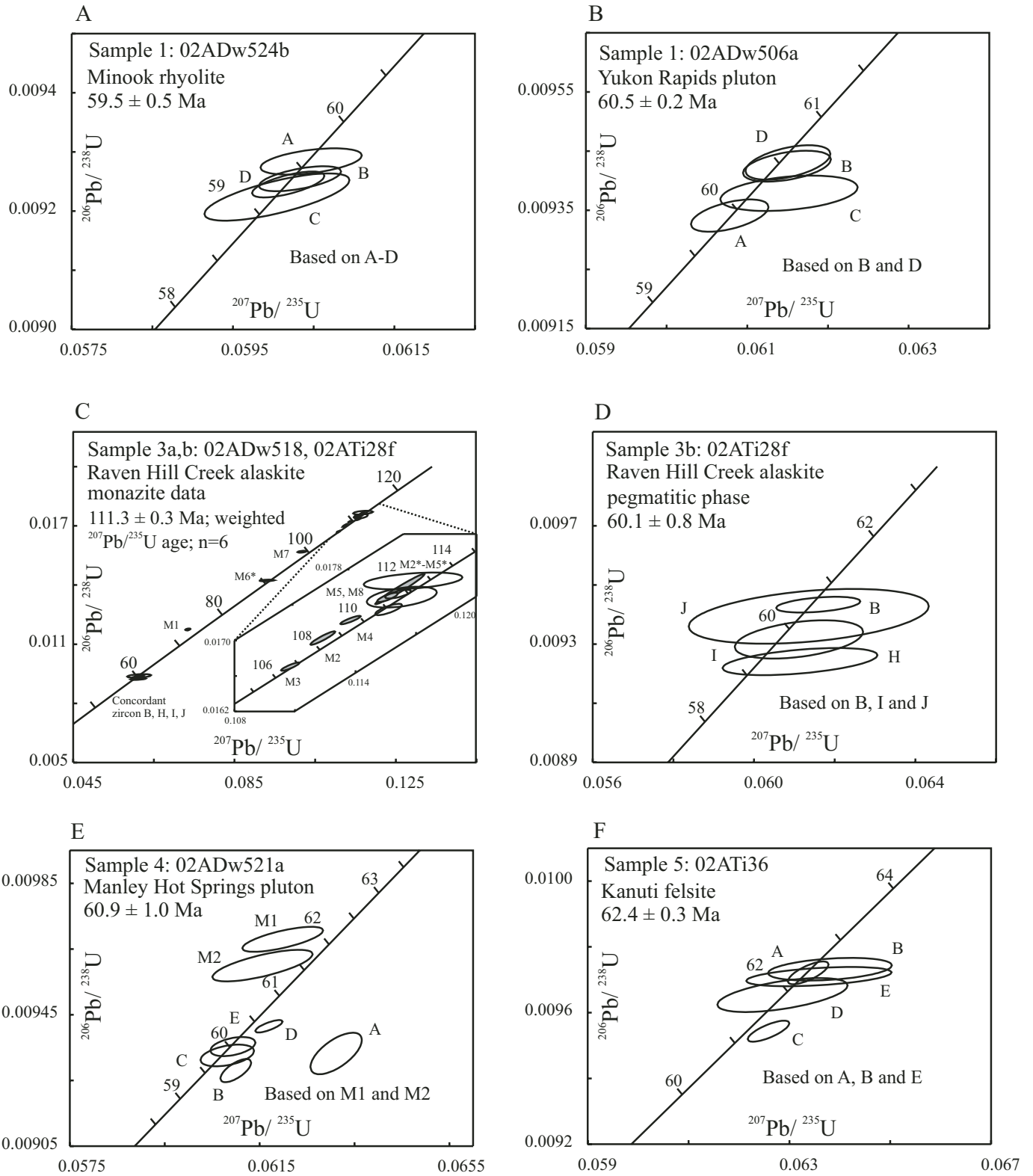


Figure 12. Concordia diagrams for U-Pb zircon analyses for igneous rocks. Monazite data from sample 3a (02ADw518) are unshaded and fraction identifiers marked with asterisks. Monazite data from sample 3b (02ATi28F) are shaded.

TABLE 3. U/Pb TIMS ANALYTICAL DATA FOR THE RAMPART AREA, CENTRAL ALASKA

Fraction*	Wt (mg)	U <sup>+</sup> (ppm)	Pb <sup>s</sup> (ppm)	<sup>206</sup> Pb/ <sup>204</sup> Pb	Pb** (pg)	Th/U <sup>††</sup>	Isotopic ratios ( $\pm 1s, \% \text{§§}$ )			Apparent ages ( $\pm 2s, \text{Ma} \text{§§}$ )		
							<sup>206</sup> Pb/ <sup>238</sup> U	<sup>207</sup> Pb/ <sup>235</sup> U	<sup>207</sup> Pb/ <sup>206</sup> Pb	<sup>206</sup> Pb/ <sup>238</sup> U	<sup>207</sup> Pb/ <sup>235</sup> U	<sup>207</sup> Pb/ <sup>206</sup> Pb
Sample 1: 02ADw524b, Minook rhyolite, 59.5 $\pm$ 0.5 Ma												
A, 8	0.081	920	9.0	1031	43	0.55	0.00928 (0.12)	0.0605 (0.52)	0.04724 (0.48)	59.6 (0.1)	59.6 (0.6)	61 (23)
B, 12	0.077	892	9.0	1126	36	0.58	0.00925 (0.11)	0.0603 (0.42)	0.04728 (0.37)	59.4 (0.1)	59.5 (0.5)	63 (17/18)
C, 18	0.100	982	10	300	204	0.60	0.00922 (0.22)	0.0600 (0.75)	0.04721 (0.61)	59.2 (0.3)	59.2 (0.9)	60 (29/30)
D, 30	0.084	1129	12	991	57	0.81	0.00925 (0.12)	0.0602 (0.37)	0.04721 (0.31)	59.3 (0.1)	59.3 (0.4)	60 (15)
Sample 2: 02ADw506a, Yukon Rapids pluton, 60.5 $\pm$ 0.2 Ma												
A, 5	0.044	396	4.4	2502	4	1.02	0.00934 (0.15)	0.0608 (0.40)	0.04719 (0.34)	59.9 (0.02)	59.9 (0.5)	59 (16)
B, 5	0.040	404	4.7	2588	4	1.23	0.00942 (0.14)	0.0616 (0.44)	0.04732 (0.40)	60.5 (0.2)	60.6 (0.5)	65 (19)
C, 6	0.043	372	4.3	1980	6	1.17	0.00938 (0.16)	0.0615 (0.69)	0.04757 (0.66)	60.2 (0.2)	60.6 (0.8)	78 (31/32)
D, 25	0.046	358	4.2	2565	4	1.20	0.00943 (0.15)	0.0615 (0.43)	0.04730 (0.38)	60.5 (0.2)	60.6 (0.5)	64 (18)
Sample 3a: 02ADw518, Raven Creek Hill alaskite; monazite only, composite age with sample 3b, below: 111.3 $\pm$ 0.3 Ma												
M2, 1	0.010	7296	297	2350	34	5.22	0.01735 (0.18)	0.1156 (0.29)	0.04834 (0.18)	110.9 (0.4)	111.1 (0.6)	115.9 (8.7)
M3, 1	0.009	3898	255	2426	16	10.23	0.01749 (0.34)	0.1163 (0.75)	0.04823 (0.67)	111.8 (0.7)	111.8 (1.7)	110 (31/32)
M4, 1	0.008	3004	224	2693	10	11.94	0.01767 (0.27)	0.1169 (1.05)	0.04796 (0.96)	112.9 (0.6)	112.2 (2.2)	97 (45/46)
M5, 1	0.006	5508	263	3077	12	6.57	0.01752 (0.14)	0.1161 (0.28)	0.04806 (0.21)	112.0 (0.3)	111.5 (0.6)	102.2 (9.8)
M6, 5	0.001	19190	868	1000	17	8.21	0.01423 (0.15)	0.0931 (1.02)	0.04740 (0.97)	91.1 (0.3)	90.3 (1.8)	69 (46/47)
Sample 3b: 02AT128f, Raven Creek Hill alaskite; monazite; composite age with sample 3a, above: 111.3 $\pm$ 0.3 Ma												
M1, 2	0.034	1553	55	4291	8	4.32	0.01175 (0.20)	0.0735 (0.44)	0.04532 (0.38)	75.3 (0.3)	72.0 (0.6)	-39 (18)
M2, 6	0.035	14704	383	4292	131	2.27	0.01703 (0.22)	0.1124 (0.27)	0.04787 (0.10)	108.9 (0.5)	108.1 (0.6)	92.6 (4.9)
M3, 6	0.038	6035	170	4622	53	2.84	0.01671 (0.14)	0.1108 (0.21)	0.04809 (0.10)	106.8 (0.3)	106.7 (0.4)	103.5 (4.8)
M4, 6	0.044	10051	325	2786	175	3.52	0.01723 (0.14)	0.1138 (0.22)	0.04788 (0.12)	110.1 (0.3)	109.4 (0.5)	93.3 (5.5)
M5, 11	0.077	11127	328	3305	292	2.79	0.01758 (0.48)	0.1162 (0.52)	0.04794 (0.11)	112.3 (1.1)	111.6 (1.1)	96.3 (5.4)
M7, 1	0.027	6511	176	2172	78	2.95	0.01569 (0.15)	0.1017 (0.54)	0.04702 (0.49)	100.4 (0.30)	98.4 (1.00)	50.3 (023/024)
M8, 1	0.008	6380	163	3955	14	2.01	0.01749 (0.15)	0.1156 (0.22)	0.04794 (0.13)	111.8 (0.3)	111.1 (0.5)	96.4 (6.3)
Sample 3b: 02AT128f, Raven Creek Hill alaskite; zircon from pegmatitic phase, 60.1 $\pm$ 0.8 Ma												
B, 8	0.032	339	3.8	1014	6	1.07	0.00943 (0.14)	0.0616 (0.85)	0.04735 (0.80)	60.5 (0.2)	60.7 (1.0)	67 (38)
H, 1	0.010	279	3.0	363	5	0.89	0.00924 (0.25)	0.0611 (1.6)	0.04798 (1.5)	59.3 (0.3)	60.3 (1.8)	98 (68/71)
I, 2	0.011	325	3.0	489	4	0.86	0.00932 (0.35)	0.0611 (1.3)	0.04757 (1.2)	59.8 (0.4)	60.2 (1.5)	78 (56/58)
J, 2	0.012	153	1.6	446	2	0.67	0.00939 (0.49)	0.0614 (2.4)	0.04737 (2.3)	60.3 (0.6)	60.5 (2.9)	68 (106/113)

(continued)

TABLE 3. U/Pb TIMS ANALYTICAL DATA FOR THE RAMPART AREA, CENTRAL ALASKA (continued)

Fraction*	Wt (mg)	U <sup>+</sup> (ppm)	Pb <sup>§</sup> (ppm)	$\frac{^{206}\text{Pb}}{^{204}\text{Pb}}$	Pb** (pg)	Th/U <sup>††</sup>	Isotopic ratios ( $\pm 1\sigma$ , %) <sup>§§</sup>			Apparent ages ( $\pm 2\sigma$ , Ma) <sup>§§</sup>		
							$^{206}\text{Pb}/^{238}\text{U}$	$^{207}\text{Pb}/^{235}\text{U}$	$^{207}\text{Pb}/^{206}\text{Pb}$	$^{206}\text{Pb}/^{238}\text{U}$	$^{207}\text{Pb}/^{235}\text{U}$	$^{207}\text{Pb}/^{206}\text{Pb}$
Sample 4: 02ADw521a, Manley Hot Springs pluton, 60.9 $\pm$ 1.0 Ma												
A, 5	0.036	1080	9.8	7540	3	0.24	0.00933 (0.34)	0.0631 (0.43)	0.04905 (0.33)	59.9 (0.4)	62.1 (0.5)	150 (16)
B, 5	0.032	1121	9.9	6108	3	0.17	0.00928 (0.19)	0.0310 (0.27)	0.04767 (0.19)	59.6 (0.2)	60.1 (0.3)	83.0 (9.2)
C, 8	0.020	502	4.5	2311	2	0.25	0.00933 (0.18)	0.0608 (0.46)	0.04730 (0.42)	59.8 (0.2)	60.0 (0.5)	64 (20)
D, 15	0.041	710	6.4	2583	7	0.22	0.00942 (0.10)	0.0617 (0.23)	0.04752 (0.17)	60.4 (0.1)	60.8 (0.3)	75.6 (8.1)
E, 30	0.032	890	7.9	2644	66	0.19	0.00935 (0.15)	0.0609 (0.39)	0.04725 (0.35)	60.0 (0.2)	60.1 (0.5)	62 (17)
M1, 2	0.031	2678	233	263	199	29.3	0.00960 (0.25)	0.0616 (0.86)	0.04651 (0.70)	61.6 (0.3)	60.7 (1.0)	24 (33/34)
M2, 4	0.027	2086	188	388	90	30.2	0.00968 (0.20)	0.0620 (0.69)	0.04645 (0.56)	62.1 (0.2)	61.1 (0.8)	21 (27)
Sample 5: 02ATI36; Kanuti felsite, 62.4 $\pm$ 0.3 Ma												
A, 5	0.041	621	6.6	1225	13	0.67	0.00972 (0.18)	0.0634 (0.32)	0.04728 (0.22)	62.4 (0.2)	62.4 (0.4)	63 (11)
B, 5	0.065	720	7.9	922	31	0.84	0.00973 (0.18)	0.0638 (0.96)	0.04755 (0.92)	62.4 (0.2)	62.8 (1.2)	77 (43/44)
C, 7	0.035	819	8.6	1067	17	0.72	0.00954 (0.17)	0.0626 (0.33)	0.04756 (0.23)	61.2 (0.2)	61.6 (0.4)	78 (11)
D, 7	0.040	422	4.4	388	28	0.69	0.00965 (0.27)	0.0629 (1.0)	0.04723 (0.90)	61.9 (0.33)	61.9 (1.2)	61 (43/44)
E, 14	0.033	381	3.9	662	12	0.57	0.00971 (0.15)	0.0636 (1.1)	0.04750 (1.1)	62.3 (0.2)	62.6 (1.4)	74 (50/52)

Note: **Grain descriptions:** **Minook rhyolite**—clear to slightly cloudy, pale tan, slightly rounded (resorbed) prisms; due to small volume of heavy minerals recovered no magnetic separation was performed. **Raven Creek Hill alkali**—zircon: clear, colorless, elongate tabular and prismatic grains up to 500  $\mu\text{m}$  in length; monazite: clear, pale yellow subhedral tables and prisms and stubby anhedral grains; **Yukon Rapids pluton**—clear, pale pink prisms up to 1000  $\mu\text{m}$  in length with aspect ratios of 5:1. **Manley Hot Springs pluton**—zircon clear to slightly cloudy, pale pink, stubby to elongate prisms; grains with c-axis parallel tubes were selected and those with visible cores were avoided; monazite clear, yellow, subhedral losenges. **Kanuti felsite**—clear, very pale yellow, euhedral elongate prisms up to 900  $\mu\text{m}$  in length; all selected grains contained c-axis parallel tubes.

\*All zircon grains selected for analysis were air abraded prior to dissolution. Fraction identifier: zircon, single letter; monazite, M followed by number. Fraction ID followed by number of grains or fragments analyzed. In general, the coarsest (>100  $\mu\text{m}$ , intermediate dimension), most nonmagnetic (nonmagnetic at 2° sideslope on Franz magnetic separator with field strength of 1.8 A) zircon grains were selected for analysis. Monazite recovered in relatively magnetic separate.

†U blank correction of 1 pg  $\pm$  20%; U fractionation corrections were measured for each run with a double  $^{233}\text{U}$ - $^{235}\text{U}$  spike.

§Radiogenic Pb

##Measured ratio corrected for spike and Pb fractionation of 0.0037–0.0032/amu  $\pm$  20% (Daly collector) which was determined by repeated analysis of NBS Pb 981 standard throughout the course of this study.

\*\*Total common Pb in analysis based on blank isotopic composition.

††Model Th/U; Th derived from radiogenic  $^{208}\text{Pb}$  and  $^{207}\text{Pb}/^{206}\text{Pb}$  age of fraction.

§§Blank and common Pb corrected; Pb procedural blanks were <3 pg and U <1 pg. Common Pb isotopic compositions are based on Stacey and Kramers (1975) model Pb at the interpreted age of the rock or the  $^{207}\text{Pb}/^{206}\text{Pb}$  age of the fraction.

TABLE 4.  $^{40}\text{Ar}/^{39}\text{Ar}$  ANALYTICAL DATA, RAMPART AREA, CENTRAL ALASKA

Laser (mW)	Cum. $^{39}\text{Ar}$	$^{40}\text{Ar}/^{39}\text{Ar}$ measured	$^{37}\text{Ar}/^{39}\text{Ar}$ measured	$^{36}\text{Ar}/^{39}\text{Ar}$ measured	% Atm. $^{40}\text{Ar}$	Ca/K	Cl/K	$^{40}\text{Ar}^*/^{39}\text{Ar}_k$	Age (Ma)
VABM Shale, 85ADO75, Biotite†									
200	0.0021	15.01 ± 0.41	0.1962 ± 0.0355	0.05 ± 0.0229	98.5	0.36 ± 0.065	0.0174 ± 0.0057	0.22 ± 6.75	0.97 ± 29.84
400	0.0052	14.5 ± 0.29	0.3197 ± 0.0226	0.0302 ± 0.0136	61.5	0.587 ± 0.041	0.0149 ± 0.0044	5.57 ± 4	24.49 ± 17.47
600	0.01	13.77 ± 0.21	0.221 ± 0.0117	0.019 ± 0.0083	40.8	0.406 ± 0.021	0.0109 ± 0.0025	8.14 ± 2.46	35.64 ± 10.66
800	0.0178	12.75 ± 0.09	0.1312 ± 0.006	0.0183 ± 0.005	42.5	0.241 ± 0.011	0.014 ± 0.0014	7.32 ± 1.47	32.07 ± 6.4
1000	0.032	14.5 ± 0.09	0.1027 ± 0.0061	0.0126 ± 0.0031	25.6	0.188 ± 0.011	0.0154 ± 0.001	10.76 ± 0.93	46.97 ± 4
1250	0.0667	14.63 ± 0.06	0.0783 ± 0.0025	0.0051 ± 0.0016	10.4	0.144 ± 0.005	0.0151 ± 0.0003	13.09 ± 0.46	56.97 ± 1.98
1500	0.1175	14.42 ± 0.04	0.0878 ± 0.0019	0.0042 ± 0.0011	8.5	0.161 ± 0.004	0.0142 ± 0.0003	13.16 ± 0.32	57.29 ± 1.39
1900	0.184	14.43 ± 0.04	0.031 ± 0.0013	0.0014 ± 0.0006	2.9	0.057 ± 0.002	0.0136 ± 0.0002	13.98 ± 0.17	60.77 ± 0.71
2400	0.2828	14.38 ± 0.03	0.0387 ± 0.0008	0.0011 ± 0.0005	2.2	0.071 ± 0.002	0.0125 ± 0.0001	14.04 ± 0.14	61.03 ± 0.61
3000	0.4533	14.23 ± 0.03	0.0415 ± 0.0005	0.0009 ± 0.0003	1.8	0.076 ± 0.001	0.0126 ± 0.0001	13.94 ± 0.08	60.62 ± 0.33
4000	0.7538	14.11 ± 0.02	0.0376 ± 0.0003	0.0006 ± 0.0002	1.3	0.069 ± 0.001	0.0136 ± 0.0001	13.9 ± 0.07	60.43 ± 0.28
9000	1.0000	14.06 ± 0.02	0.1111 ± 0.0004	0.0005 ± 0.0002	1.0	0.204 ± 0.001	0.0135 ± 0.0001	13.9 ± 0.06	60.45 ± 0.26
Integrated		14.2 ± 0.01	0.0637 ± 0.0003	0.0017 ± 0.0002	3.4	0.117 ± 0.001	0.0134 ± 0.0001	13.68 ± 0.05	59.51 ± 0.3
VABM Shale, 85ADO75, White mica†									
300	0.0088	14.22 ± 0.2	0.0274 ± 0.0403	0.0239 ± 0.0103	49.7	0.05 ± 0.074	0.0087 ± 0.0021	7.13 ± 3.06	31.26 ± 13.28
600	0.031	14.86 ± 0.12	-0.0306 ± 0.0279	0.0001 ± 0.0084	0.3	-0.056 ± 0.051	0.0046 ± 0.002	14.8 ± 2.49	64.27 ± 10.61
900	0.0875	15.71 ± 0.04	0.0049 ± 0.0069	0.003 ± 0.0023	5.7	0.009 ± 0.013	0.0012 ± 0.0004	14.79 ± 0.69	64.24 ± 2.94
1200	0.1816	15.13 ± 0.03	0.0074 ± 0.0042	0.0022 ± 0.0013	4.3	0.014 ± 0.008	0.0005 ± 0.0004	14.45 ± 0.39	62.81 ± 1.65
1500	0.2929	14.63 ± 0.02	0.0042 ± 0.0027	0.0003 ± 0.0007	0.7	0.008 ± 0.005	0.0005 ± 0.0003	14.51 ± 0.2	63.04 ± 0.83
1800	0.3962	15.15 ± 0.02	0.0096 ± 0.003	0.0029 ± 0.0007	5.7	0.018 ± 0.005	0.0009 ± 0.0003	14.27 ± 0.22	62.01 ± 0.92
2100	0.4925	14.59 ± 0.02	0.0227 ± 0.0027	0.0009 ± 0.0008	1.9	0.042 ± 0.005	0.0004 ± 0.0003	14.29 ± 0.23	62.12 ± 0.99
2500	0.598	14.49 ± 0.02	0.0151 ± 0.002	0.0011 ± 0.0005	2.2	0.028 ± 0.004	0.0012 ± 0.0003	14.14 ± 0.15	61.46 ± 0.64
3000	0.7385	14.32 ± 0.02	0.009 ± 0.0011	-0.0001 ± 0.0004	-0.2	0.017 ± 0.002	0.0006 ± 0.0003	14.33 ± 0.11	62.27 ± 0.47
4000	0.9196	14.26 ± 0.03	0.0133 ± 0.001	0.0006 ± 0.0005	1.3	0.024 ± 0.002	0.0008 ± 0.0001	14.05 ± 0.16	61.08 ± 0.68
5000	0.9924	14.24 ± 0.06	0.0259 ± 0.0048	0.0017 ± 0.0033	3.6	0.047 ± 0.009	0.0008 ± 0.0003	13.7 ± 0.98	59.59 ± 4.21
9000	1.0000	15.69 ± 0.19	-0.0144 ± 0.0176	-0.0018 ± 0.0057	-3.3	-0.026 ± 0.032	-0.001 ± 0.0021	16.18 ± 1.69	70.18 ± 7.19
Integrated		14.64 ± 0.01	0.0112 ± 0.0011	0.0013 ± 0.0004	2.7	0.021 ± 0.002	0.0009 ± 0.0001	14.22 ± 0.12	61.81 ± 0.56
Senatis, 02RSR13B, Biotite†									
300	0.0055	14.26 ± 0.17	0.1041 ± 0.0324	0.0196 ± 0.0112	40.6	0.191 ± 0.06	0.013 ± 0.0038	8.45 ± 3.3	36.97 ± 14.29
600	0.0277	10.18 ± 0.03	0.1145 ± 0.0223	0.0064 ± 0.0092	18.5	0.21 ± 0.041	0.0096 ± 0.0015	8.28 ± 2.71	36.23 ± 11.75
900	0.0753	12.15 ± 0.03	0.0784 ± 0.0039	0.0021 ± 0.001	5.1	0.144 ± 0.007	0.0092 ± 0.0004	11.51 ± 0.3	50.18 ± 1.29
1200	0.1335	14.69 ± 0.04	0.0513 ± 0.003	0.0007 ± 0.0009	1.3	0.094 ± 0.005	0.01 ± 0.0003	14.47 ± 0.26	62.87 ± 1.13
1500	0.2023	14.97 ± 0.04	0.0187 ± 0.0017	0.0001 ± 0.0009	0.2	0.034 ± 0.003	0.0096 ± 0.0004	14.92 ± 0.26	64.8 ± 1.12
1800	0.2849	15.35 ± 0.03	0.0219 ± 0.0066	0.0008 ± 0.0017	1.4	0.04 ± 0.012	0.0102 ± 0.0004	15.1 ± 0.51	65.56 ± 2.19
2100	0.3955	15.27 ± 0.02	0.0152 ± 0.0011	-0.0003 ± 0.0006	-0.5	0.028 ± 0.002	0.0119 ± 0.0001	15.32 ± 0.18	66.51 ± 0.76
2500	0.5312	14.75 ± 0.02	0.0207 ± 0.001	0.0004 ± 0.0005	0.7	0.038 ± 0.002	0.0126 ± 0.0001	14.62 ± 0.16	63.5 ± 0.67
3000	0.6878	14.45 ± 0.04	0.0218 ± 0.0014	-0.0002 ± 0.001	-0.3	0.04 ± 0.003	0.0121 ± 0.0001	14.47 ± 0.31	62.87 ± 1.33
4000	0.8256	14.97 ± 0.02	0.0255 ± 0.0007	0.0005 ± 0.0005	1.0	0.047 ± 0.001	0.0114 ± 0.0001	14.8 ± 0.16	64.27 ± 0.67
5000	0.9172	15.27 ± 0.02	0.0153 ± 0.0022	0.0005 ± 0.0004	0.9	0.028 ± 0.004	0.0108 ± 0.0005	15.1 ± 0.12	65.58 ± 0.5
9000	1.0000	15.78 ± 0.02	0.0193 ± 0.0013	0.0011 ± 0.0008	2	0.035 ± 0.002	0.011 ± 0.0001	15.43 ± 0.25	66.97 ± 1.06
Integrated		14.76 ± 0.01	0.0273 ± 0.0009	0.0007 ± 0.0004	1.3	0.05 ± 0.002	0.0112 ± 0.0001	14.54 ± 0.1	63.16 ± 0.5

(continued)

TABLE 4.  $^{40}\text{Ar}/^{39}\text{Ar}$  ANALYTICAL DATA, RAMPART AREA, CENTRAL ALASKA (continued)

Laser (mW)	Cum. $^{39}\text{Ar}$	$^{40}\text{Ar}/^{39}\text{Ar}$ measured	$^{37}\text{Ar}/^{39}\text{Ar}$ measured	$^{36}\text{Ar}/^{39}\text{Ar}$ measured	% Atm. $^{40}\text{Ar}$	Ca/K	Cl/K	$^{40}\text{Ar}^*/^{39}\text{Ar}_k$	Age (Ma)
NW Silver, 02AT112C, Whole rock, Biotite <sup>s</sup>									
300	0.017	14.274 ± 0.27	0.219 ± 0.021	0.0397 ± 0.0018	82.3	0.401 ± 0.039	0.0000 ± 0.0005	2.53 ± 0.54	11.41 ± 2.44
500	0.05	8.262 ± 0.124	0.202 ± 0.013	0.0122 ± 0.0018	43.6	0.371 ± 0.024	-0.0001 ± 0.0003	4.64 ± 0.52	20.92 ± 2.34
700	0.104	13.655 ± 0.169	0.417 ± 0.008	0.006 ± 0.0007	12.8	0.765 ± 0.015	0.0004 ± 0.0003	11.89 ± 0.27	53.09 ± 1.17
900	0.186	14.576 ± 0.079	0.423 ± 0.005	0.0032 ± 0.0004	6.2	0.777 ± 0.01	0.0004 ± 0.0001	13.65 ± 0.14	60.81 ± 0.63
1100	0.231	14.912 ± 0.071	0.735 ± 0.011	0.0053 ± 0.0008	10.1	1.349 ± 0.021	0.0002 ± 0.0002	13.39 ± 0.26	59.69 ± 1.12
1300	0.275	14.665 ± 0.072	0.524 ± 0.01	0.0065 ± 0.0007	12.9	0.961 ± 0.018	0.0001 ± 0.0002	12.75 ± 0.22	56.86 ± 0.98
1500	0.334	14.207 ± 0.077	0.272 ± 0.014	0.0024 ± 0.001	4.8	0.5 ± 0.027	0.0007 ± 0.0002	13.5 ± 0.3	60.14 ± 1.3
1700	0.402	14.073 ± 0.036	0.166 ± 0.013	0.0022 ± 0.0007	4.6	0.305 ± 0.024	0.0001 ± 0.0002	13.4 ± 0.2	59.71 ± 0.88
1900	0.483	14.15 ± 0.055	0.127 ± 0.01	0.0018 ± 0.0005	3.7	0.234 ± 0.018	0.0003 ± 0.0002	13.6 ± 0.17	60.58 ± 0.74
2100	0.574	14.444 ± 0.046	0.112 ± 0.009	0.0022 ± 0.0005	4.5	0.205 ± 0.017	0.0003 ± 0.0001	13.77 ± 0.14	61.32 ± 0.62
2500	0.724	14.315 ± 0.106	0.115 ± 0.005	0.0013 ± 0.0003	2.6	0.211 ± 0.01	0.0003 ± 0.0001	13.92 ± 0.13	61.98 ± 0.59
3000	0.887	14.189 ± 0.096	0.179 ± 0.005	0.0014 ± 0.0003	2.7	0.329 ± 0.009	0.0004 ± 0.0001	13.78 ± 0.12	61.38 ± 0.54
4000	0.974	14.106 ± 0.058	0.437 ± 0.009	0.0013 ± 0.0005	2.6	0.802 ± 0.017	0.0002 ± 0.0001	13.72 ± 0.16	61.13 ± 0.69
9000	1.0000	14.335 ± 0.1	1.881 ± 0.035	0.0073 ± 0.0022	14.1	3.455 ± 0.065	-0.0001 ± 0.0007	12.31 ± 0.66	54.94 ± 2.88
Integrated		14.08 ± 0.028	0.305 ± 0.003	0.0036 ± 0.0002	7.3	0.561 ± 0.005	0.0003 ± 0.0001	13.03 ± 0.06	58.09 ± 0.28
Main Minook, 02AT123, White mica <sup>s</sup>									
250	0.002	43.599 ± 4.562	-1.118 ± 1.035	0.3677 ± 0.1071	249.6	-2.049 ± 1.896	0.0148 ± 0.0401	-65.12 ± 30.3	-322.25 ± 164.14
500	0.013	21.433 ± 0.367	-0.054 ± 0.19	0.1032 ± 0.0146	142.5	-0.1 ± 0.348	0.008 ± 0.0065	-9.1 ± 4.29	-41.72 ± 19.88
750	0.039	15.667 ± 0.252	-0.049 ± 0.12	0.0411 ± 0.0087	77.6	-0.091 ± 0.22	0.0029 ± 0.0036	3.5 ± 2.57	15.8 ± 11.53
1000	0.106	14.491 ± 0.12	0.048 ± 0.038	0.0205 ± 0.004	41.9	0.088 ± 0.069	0.0019 ± 0.0017	8.41 ± 1.19	37.7 ± 5.28
1250	0.204	14.63 ± 0.057	0.077 ± 0.035	0.0243 ± 0.0035	49.2	0.142 ± 0.064	0.0033 ± 0.001	7.42 ± 1.04	33.29 ± 4.63
1500	0.302	14.073 ± 0.066	0.007 ± 0.022	0.0156 ± 0.0022	32.7	0.013 ± 0.041	0.0011 ± 0.0008	9.45 ± 0.64	42.31 ± 2.84
1750	0.411	13.468 ± 0.052	0.017 ± 0.011	0.0028 ± 0.0015	6.1	0.031 ± 0.02	0.0016 ± 0.0003	12.62 ± 0.44	56.31 ± 1.91
2000	0.507	13.898 ± 0.05	0.023 ± 0.011	0.0029 ± 0.0016	6.2	0.042 ± 0.021	0.0012 ± 0.0004	13.02 ± 0.47	58.04 ± 2.06
2500	0.6	13.438 ± 0.052	0.03 ± 0.011	0.004 ± 0.0015	8.7	0.055 ± 0.02	0.0019 ± 0.0003	12.24 ± 0.45	54.64 ± 1.97
3000	0.675	13.325 ± 0.056	0.043 ± 0.017	-0.0007 ± 0.0019	-1.5	0.079 ± 0.031	0.0023 ± 0.0004	13.5 ± 0.56	60.17 ± 2.46
4000	0.806	13.568 ± 0.052	0.023 ± 0.012	0.0021 ± 0.0014	4.7	0.042 ± 0.022	0.0006 ± 0.0004	12.91 ± 0.41	57.56 ± 1.8
5000	0.878	13.682 ± 0.066	0.102 ± 0.027	0.0063 ± 0.0031	13.6	0.187 ± 0.049	0.0018 ± 0.0007	11.8 ± 0.92	52.68 ± 4.06
9000	1.0000	13.654 ± 0.09	0.029 ± 0.008	0.0024 ± 0.0012	5.1	0.054 ± 0.015	0.001 ± 0.0002	12.93 ± 0.37	57.67 ± 1.63
Integrated		13.987 ± 0.022	0.032 ± 0.007	0.0101 ± 0.0007	21.3	0.058 ± 0.013	0.0017 ± 0.0002	10.99 ± 0.22	49.11 ± 0.97

(continued)

TABLE 4.  $^{40}\text{Ar}/^{39}\text{Ar}$  ANALYTICAL DATA, RAMPART AREA, CENTRAL ALASKA (continued)

Laser (mW)	Cum. $^{39}\text{Ar}$	$^{40}\text{Ar}/^{39}\text{Ar}$ measured	$^{37}\text{Ar}/^{39}\text{Ar}$ measured	$^{36}\text{Ar}/^{39}\text{Ar}$ measured	% Atm. $^{40}\text{Ar}$	Ca/K	Cl/K	$^{40}\text{Ar}^*/^{39}\text{Ar}_k$	Age (Ma)
Raven Creek Hill, 02ATI27G, Biotite†									
200	0.0022	22.66 ± 4.56	-0.2324 ± 0.2055	-0.1953 ± 0.1602	-255.0	-0.426 ± 0.377	-0.0252 ± 0.0493	80.31 ± 48.64	324.16 ± 179.7
400	0.0065	35.83 ± 4.3	-0.0896 ± 0.1203	0.0273 ± 0.0904	22.5	-0.164 ± 0.221	0.0208 ± 0.0273	27.74 ± 26.91	118.67 ± 111.42
600	0.0155	28.5 ± 1.61	0.0331 ± 0.0637	0.0117 ± 0.0427	12.1	0.061 ± 0.117	0.0087 ± 0.0127	25.03 ± 12.7	107.42 ± 52.93
800	0.0408	26.26 ± 0.47	0.0272 ± 0.0204	0.0107 ± 0.0123	12.0	0.05 ± 0.037	0.0051 ± 0.0042	23.07 ± 3.67	99.23 ± 15.36
1000	0.1481	21.64 ± 0.39	0.0121 ± 0.0112	0.0121 ± 0.0059	16.6	0.022 ± 0.02	0.0054 ± 0.0024	18.02 ± 1.77	77.98 ± 7.48
1250	0.2577	22.05 ± 0.38	0.0119 ± 0.0121	0.0114 ± 0.0061	15.3	0.022 ± 0.022	0.0038 ± 0.0024	18.65 ± 1.82	80.63 ± 7.69
1500	0.3435	22.78 ± 0.48	0.0169 ± 0.0144	0.0095 ± 0.0076	12.4	0.031 ± 0.026	0.0054 ± 0.0029	19.94 ± 2.27	86.09 ± 9.57
1900	0.4477	22.4 ± 0.4	0.0193 ± 0.0121	0.0184 ± 0.0062	24.3	0.035 ± 0.022	0.0053 ± 0.0025	16.94 ± 1.85	73.39 ± 7.85
2400	0.5733	22.53 ± 0.08	0.0054 ± 0.0062	0.0048 ± 0.0033	6.3	0.01 ± 0.011	0.0026 ± 0.0008	21.08 ± 0.99	90.88 ± 4.16
3000	0.6994	22.14 ± 0.11	0.0036 ± 0.0048	0.0064 ± 0.0028	8.6	0.007 ± 0.009	0.0019 ± 0.0009	20.21 ± 0.82	87.25 ± 3.46
4000	0.8664	23.48 ± 0.11	0.008 ± 0.0036	0.0086 ± 0.0026	10.8	0.015 ± 0.007	0.0014 ± 0.0007	20.92 ± 0.77	90.22 ± 3.23
9000	1.0000	25.01 ± 0.12	0.0121 ± 0.0078	0.0108 ± 0.0038	12.8	0.022 ± 0.014	0.0018 ± 0.0008	21.78 ± 1.12	93.83 ± 4.7
Integrated		23.03 ± 0.09	0.0102 ± 0.0031	0.0096 ± 0.0017	12.4	0.019 ± 0.006	0.0033 ± 0.0006	20.16 ± 0.51	87.02 ± 2.18
96RN110a, White mica†									
100	0.0038	6.168 ± 0.0903	0.00813 ± 0.00552	0.01748 ± 0.00153	78.4	0.0149 ± 0.0101	0.00106 ± 0.0003	1.4236 ± 0.4539	19.4 ± 6.2
150	0.0074	7.1602 ± 0.0837	0.02289 ± 0.00708	0.01531 ± 0.00064	63.4	0.042 ± 0.013	0.00133 ± 0.00021	2.6093 ± 0.2014	35.4 ± 2.7
200	0.013	7.0406 ± 0.0758	0.01098 ± 0.00843	0.01123 ± 0.00065	47.3	0.0202 ± 0.0155	0.0006 ± 0.00028	3.6947 ± 0.1993	49.9 ± 2.7
300	0.0263	6.3533 ± 0.0406	0.00865 ± 0.00203	0.00677 ± 0.00029	31.6	0.0159 ± 0.0037	0.00064 ± 0.00012	4.326 ± 0.0921	58.3 ± 1.2
450	0.0684	5.1744 ± 0.0311	0.0036 ± 0.00056	0.00167 ± 0.00007	9.6	0.0066 ± 0.001	0.00041 ± 0.00005	4.6531 ± 0.0365	62.7 ± 0.5
600	0.1186	5.1902 ± 0.0181	0.00381 ± 0.00037	0.00198 ± 0.00009	11.3	0.007 ± 0.0007	0.00036 ± 0.00008	4.5766 ± 0.0301	61.7 ± 0.4
750	0.1698	5.1392 ± 0.0192	0.00377 ± 0.00054	0.0021 ± 0.0001	12.1	0.0069 ± 0.001	0.00046 ± 0.00006	4.4904 ± 0.0342	60.5 ± 0.5
900	0.2127	5.2433 ± 0.0267	0.00738 ± 0.0003	0.00251 ± 0.00009	14.2	0.0135 ± 0.0006	0.00038 ± 0.00006	4.4739 ± 0.0364	60.3 ± 0.5
1050	0.2637	5.0891 ± 0.0218	0.00726 ± 0.00065	0.00157 ± 0.00007	9.1	0.0133 ± 0.0012	0.00038 ± 0.00003	4.5985 ± 0.0298	62 ± 0.4
1200	0.3234	4.8949 ± 0.029	0.00561 ± 0.00033	0.00082 ± 0.00006	4.9	0.0103 ± 0.0006	0.0003 ± 0.00004	4.6255 ± 0.0326	62.3 ± 0.4
1350	0.3938	4.7877 ± 0.0195	0.00669 ± 0.00041	0.00032 ± 0.0001	2.0	0.0123 ± 0.0007	0.00038 ± 0.00003	4.6636 ± 0.0358	62.8 ± 0.5
1500	0.4739	4.7281 ± 0.0092	0.00795 ± 0.0003	0.00034 ± 0.00007	2.1	0.0146 ± 0.0005	0.0003 ± 0.00005	4.5994 ± 0.0239	62 ± 0.3
1650	0.5647	4.7599 ± 0.0113	0.00933 ± 0.00048	0.00041 ± 0.00007	2.6	0.0171 ± 0.0009	0.00038 ± 0.00004	4.6097 ± 0.0234	62.1 ± 0.3
1800	0.6466	4.7864 ± 0.0113	0.01577 ± 0.00041	0.00052 ± 0.00008	3.2	0.0289 ± 0.0008	0.00038 ± 0.00004	4.6065 ± 0.0267	62.1 ± 0.4
2000	0.7412	4.7011 ± 0.0197	0.01006 ± 0.00066	0.00052 ± 0.00008	3.3	0.0185 ± 0.0012	0.00036 ± 0.00003	4.5202 ± 0.031	60.9 ± 0.4
3500	0.9827	4.7178 ± 0.0267	0.01733 ± 0.00034	0.00067 ± 0.00002	4.2	0.0318 ± 0.0006	0.00041 ± 0.00003	4.4919 ± 0.0276	60.5 ± 0.4
8500	1.0000	5.3387 ± 0.0382	0.01799 ± 0.00233	0.00246 ± 0.00035	13.7	0.033 ± 0.0043	0.00045 ± 0.00013	4.5838 ± 0.1093	61.8 ± 1.5
Integrated		4.9095 ± 0.0077	0.01054 ± 0.00015	0.00117 ± 0.00002	7.1	0.0194 ± 0.0003	0.00039 ± 0.00001	4.5354 ± 0.0099	61.1 ± 0.2

(continued)

TABLE 4.  $^{40}\text{Ar}/^{39}\text{Ar}$  ANALYTICAL DATA, RAMPART AREA, CENTRAL ALASKA (continued)

Laser (mW)	Cum. $^{39}\text{Ar}$	$^{40}\text{Ar}/^{39}\text{Ar}$ measured	$^{37}\text{Ar}/^{39}\text{Ar}$ measured	$^{36}\text{Ar}/^{39}\text{Ar}$ measured	% Atm. $^{40}\text{Ar}$	Ca/K	Cl/K	$^{40}\text{Ar}^*/^{39}\text{Ar}_k$	Age (Ma)
96RN191 White mica#									
100	0.0128	3.4159 ± 0.0216	0.01621 ± 0.00325	0.0024 ± 0.00055	20.9	0.0297 ± 0.006	0.00199 ± 0.00022	2.6801 ± 0.1631	36.4 ± 2.2
200	0.0673	5.5371 ± 0.0204	0.00435 ± 0.00079	0.00083 ± 0.00014	4.4	0.008 ± 0.0014	0.00217 ± 0.0001	5.265 ± 0.045	70.8 ± 0.6
300	0.1529	4.9619 ± 0.0214	0.00178 ± 0.00053	0.00014 ± 0.0001	0.9	0.0033 ± 0.001	0.00246 ± 0.00006	4.8907 ± 0.0368	65.8 ± 0.5
500	0.2787	4.763 ± 0.0197	0.00042 ± 0.00048	0.00064 ± 0.00005	4.0	0.0008 ± 0.0009	0.00338 ± 0.0001	4.5463 ± 0.0254	61.3 ± 0.3
700	0.4155	4.8262 ± 0.0259	0.00006 ± 0.00037	0.00101 ± 0.00011	6.2	0.0001 ± 0.0007	0.00247 ± 0.00005	4.4992 ± 0.0398	60.6 ± 0.5
900	0.5477	4.6114 ± 0.0159	-0.0013 ± 0.00065	0.00008 ± 0.00007	0.5	-0.0024 ± 0.0012	0.00211 ± 0.00005	4.5598 ± 0.0257	61.4 ± 0.3
1050	0.6654	4.6451 ± 0.0091	-0.0015 ± 0.00037	0.00024 ± 0.00007	1.6	-0.0028 ± 0.0012	0.00229 ± 0.00003	4.5444 ± 0.0224	61.2 ± 0.3
1200	0.7336	4.5697 ± 0.0218	-0.0007 ± 0.00121	0.00002 ± 0.00011	0.1	-0.0013 ± 0.0022	0.00162 ± 0.00005	4.5359 ± 0.0391	61.1 ± 0.5
1350	0.7578	4.5391 ± 0.0335	-0.0065 ± 0.0023	-0.00048 ± 0.00029	-3.2	-0.012 ± 0.0042	0.00216 ± 0.00012	4.653 ± 0.0935	62.7 ± 1.2
1500	0.7695	4.5717 ± 0.0332	-0.0059 ± 0.00388	-0.0008 ± 0.00062	-5.2	-0.0107 ± 0.0071	0.00257 ± 0.00026	4.7776 ± 0.1858	64.3 ± 2.5
2000	0.8243	4.5348 ± 0.0182	-0.0009 ± 0.001	0.00016 ± 0.00014	1.0	-0.0017 ± 0.0018	0.00176 ± 0.00009	4.459 ± 0.0462	60.1 ± 0.6
2500	0.836	4.5725 ± 0.0355	0.00349 ± 0.00459	0.00051 ± 0.00107	3.3	0.0064 ± 0.0084	0.00248 ± 0.00016	4.3925 ± 0.319	59.2 ± 4.2
2800	1.0000	4.6095 ± 0.0167	-0.0001 ± 0.0003	0.00005 ± 0.00005	0.3	-0.0002 ± 0.0006	0.00112 ± 0.00005	4.5668 ± 0.0219	61.5 ± 0.3
Integrated		4.7188 ± 0.0064	0.0000 ± 0.0002	0.00035 ± 0.00003	2.2	0.0000 ± 0.0004	0.00217 ± 0.00002	4.5874 ± 0.0114	61.8 ± 0.3
96RN16 Biotite#									
100	0.0019	84.3524 ± 0.6222	0.08072 ± 0.02111	0.28177 ± 0.00327	98.7	0.1481 ± 0.0387	0.02638 ± 0.00098	1.0674 ± 0.7938	14.6 ± 10.8
200	0.0087	15.7305 ± 0.0707	0.02507 ± 0.00473	0.04178 ± 0.00118	78.6	0.046 ± 0.0087	0.02921 ± 0.0006	3.3564 ± 0.3483	45.4 ± 4.7
300	0.0434	6.4483 ± 0.0231	0.00574 ± 0.00114	0.0077 ± 0.00016	35.5	0.0105 ± 0.0021	0.02635 ± 0.00016	4.1434 ± 0.0493	55.9 ± 0.7
450	0.0874	5.802 ± 0.0202	0.005 ± 0.00093	0.00528 ± 0.00012	27.0	0.0092 ± 0.0017	0.02624 ± 0.00019	4.2148 ± 0.0389	56.9 ± 0.5
600	0.2157	6.0573 ± 0.0087	0.0124 ± 0.00025	0.00605 ± 0.00006	29.6	0.0228 ± 0.0005	0.02562 ± 0.0001	4.2413 ± 0.0191	57.2 ± 0.3
750	0.3041	5.7037 ± 0.0132	0.01388 ± 0.00057	0.00474 ± 0.0001	24.7	0.0255 ± 0.001	0.02714 ± 0.00014	4.2755 ± 0.0313	57.7 ± 0.4
900	0.4417	5.4276 ± 0.0207	0.02887 ± 0.00068	0.00348 ± 0.00007	19.0	0.053 ± 0.0013	0.02771 ± 0.00013	4.3717 ± 0.0258	59 ± 0.3
1050	0.6007	4.9725 ± 0.0105	0.06279 ± 0.00097	0.00212 ± 0.00003	12.6	0.1152 ± 0.0018	0.02722 ± 0.00018	4.3231 ± 0.0139	58.3 ± 0.2
1200	0.709	4.72 ± 0.0199	0.10772 ± 0.00091	0.00115 ± 0.00004	7.1	0.1977 ± 0.0017	0.02754 ± 0.00019	4.36 ± 0.0226	58.8 ± 0.3
1350	0.8401	4.6436 ± 0.0156	0.10448 ± 0.00103	0.00094 ± 0.00007	5.9	0.1917 ± 0.0019	0.02781 ± 0.00011	4.3439 ± 0.0256	58.6 ± 0.3
1500	0.8965	4.6145 ± 0.0163	0.06487 ± 0.00191	0.00059 ± 0.0001	3.7	0.119 ± 0.0035	0.02979 ± 0.00017	4.4179 ± 0.0342	59.6 ± 0.5
1800	0.9885	4.4822 ± 0.0138	0.0497 ± 0.00075	0.00043 ± 0.00004	2.8	0.0912 ± 0.0014	0.02991 ± 0.00011	4.3305 ± 0.0188	58.4 ± 0.3
2200	0.9969	4.4136 ± 0.0181	0.31839 ± 0.00862	-0.00023 ± 0.00037	-2.1	0.5843 ± 0.0158	0.0248 ± 0.00058	4.4779 ± 0.1098	60.4 ± 1.5
8500	1.0000	7.9843 ± 0.0597	0.12516 ± 0.01038	0.01224 ± 0.00113	45.3	0.2297 ± 0.0191	0.02421 ± 0.00061	4.3484 ± 0.3361	58.6 ± 4.5
Integrated		5.4191 ± 0.0053	0.05418 ± 0.0003	0.00369 ± 0.00002	20.1	0.0994 ± 0.0006	0.02749 ± 0.00005	4.3055 ± 0.0084	58.1 ± 0.2

(continued)

TABLE 4. <sup>40</sup>Ar/<sup>39</sup>Ar ANALYTICAL DATA, RAMPART AREA, CENTRAL ALASKA (continued)

Laser (mW)	Cum. <sup>39</sup> Ar	<sup>40</sup> Ar/ <sup>39</sup> Ar measured	<sup>37</sup> Ar/ <sup>39</sup> Ar measured	<sup>36</sup> Ar/ <sup>39</sup> Ar measured	% Atm. <sup>40</sup> Ar	Ca/K	Cl/K	<sup>40</sup> Ar/ <sup>39</sup> Ar <sub>k</sub>	Age (Ma)
96RN244 White mica <sup>#</sup>									
100	0.0006	39.5094 ± 1.0881	0.0491 ± 0.06662	0.11422 ± 0.00965	85.5	0.0901 ± 0.1223	0.00768 ± 0.00254	5.7335 ± 2.7557	76.9 ± 36.2
200	0.0016	34.5875 ± 0.8061	0.08654 ± 0.03131	0.10432 ± 0.00549	89.2	0.1588 ± 0.0575	0.00258 ± 0.00138	3.7391 ± 1.4953	50.5 ± 19.9
300	0.0033	17.7119 ± 0.2731	0.01862 ± 0.02471	0.03809 ± 0.00332	63.6	0.0342 ± 0.0453	0.00114 ± 0.00076	6.4291 ± 0.9925	86 ± 13
450	0.0079	13.2714 ± 0.1573	0.01599 ± 0.01018	0.02505 ± 0.00096	55.9	0.0293 ± 0.0187	0.00088 ± 0.00035	5.8429 ± 0.2877	78.4 ± 3.8
600	0.0143	13.1248 ± 0.0795	0.00861 ± 0.00543	0.02217 ± 0.00056	50.0	0.0158 ± 0.01	0.00104 ± 0.00034	6.5442 ± 0.1818	87.5 ± 2.4
750	0.0279	7.7296 ± 0.0323	-0.0059 ± 0.00229	0.00444 ± 0.00036	17.0	-0.0108 ± 0.0042	0.00039 ± 0.00012	6.389 ± 0.1102	86.5 ± 1.4
900	0.0596	5.9824 ± 0.0343	-0.0019 ± 0.00106	0.00038 ± 0.00011	1.9	-0.0035 ± 0.002	0.00046 ± 0.00005	5.8419 ± 0.0464	78.3 ± 0.6
1050	0.098	7.0366 ± 0.0276	-0.0018 ± 0.00105	0.00407 ± 0.00015	17.1	-0.0033 ± 0.0019	0.00066 ± 0.00005	5.8064 ± 0.0503	77.9 ± 0.7
1200	0.1829	6.6208 ± 0.029	-0.0019 ± 0.00045	0.00111 ± 0.00007	5.0	-0.0036 ± 0.0008	0.00042 ± 0.00005	6.2625 ± 0.0343	83.9 ± 0.5
1350	0.2206	6.1601 ± 0.0173	0.00204 ± 0.00099	-0.0001 ± 0.00011	-0.5	0.0038 ± 0.0018	0.00055 ± 0.00004	6.1615 ± 0.0379	82.5 ± 0.5
1500	0.2438	6.2709 ± 0.0405	-0.0005 ± 0.00125	0.0003 ± 0.00023	1.4	-0.0009 ± 0.0023	0.00049 ± 0.00009	6.1544 ± 0.0794	82.4 ± 1
1800	0.3514	7.4686 ± 0.0161	-0.0006 ± 0.00031	0.00365 ± 0.00007	14.5	-0.0012 ± 0.0006	0.00044 ± 0.00003	6.3621 ± 0.0261	85.2 ± 0.3
2200	0.4539	6.4448 ± 0.0175	-0.0012 ± 0.00033	0.00056 ± 0.00007	2.6	-0.0021 ± 0.0006	0.00049 ± 0.00004	6.2491 ± 0.0259	83.7 ± 0.3
8500	0.8223	6.592 ± 0.0186	-0.0003 ± 0.0001	0.00132 ± 0.00003	5.9	-0.0006 ± 0.0002	0.00041 ± 0.00002	6.1731 ± 0.02	82.7 ± 0.3
9000	1.0000	7.0115 ± 0.0671	0.00657 ± 0.00026	0.00253 ± 0.00006	10.7	0.0121 ± 0.0005	0.00053 ± 0.00002	6.2345 ± 0.0663	83.5 ± 0.9
Integrated		6.8763 ± 0.0143	0.00082 ± 0.00014	0.00221 ± 0.00002	9.5	0.0015 ± 0.0003	0.00048 ± 0.00001	6.196 ± 0.0155	83 ± 0.3
96RN243a Biotite <sup>#</sup>									
100	0.013	7.3928 ± 0.0918	0.02645 ± 0.00462	0.01183 ± 0.00056	47.4	0.0485 ± 0.0085	0.02803 ± 0.00056	3.8717 ± 0.1744	52.3 ± 2.3
200	0.0966	4.7435 ± 0.0277	0.00302 ± 0.00059	0.00098 ± 0.00007	6.2	0.0055 ± 0.0011	0.02913 ± 0.00033	4.4248 ± 0.0336	59.7 ± 0.5
300	0.2213	4.5801 ± 0.0145	0.00242 ± 0.00044	0.0005 ± 0.00009	3.3	0.0044 ± 0.0008	0.02896 ± 0.00011	4.4034 ± 0.0295	59.4 ± 0.4
500	0.3774	4.5365 ± 0.0178	0.00415 ± 0.00055	0.00018 ± 0.00004	1.2	0.0076 ± 0.001	0.02669 ± 0.00014	4.4554 ± 0.0215	60.1 ± 0.3
700	0.5553	4.5227 ± 0.019	0.00357 ± 0.00035	0.00008 ± 0.00003	0.5	0.0066 ± 0.0006	0.026 ± 0.00014	4.4703 ± 0.0213	60.3 ± 0.3
900	0.5695	4.4991 ± 0.0346	-0.0023 ± 0.00446	-0.00039 ± 0.00038	-2.6	0.0041 ± 0.0082	0.02744 ± 0.0006	4.5858 ± 0.117	61.8 ± 1.6
1050	0.5741	4.5576 ± 0.0432	-0.0092 ± 0.01515	0.00043 ± 0.0009	2.8	0.0168 ± 0.0278	0.02913 ± 0.00055	4.4023 ± 0.2707	59.4 ± 3.6
1200	0.5817	4.4635 ± 0.0387	-0.0036 ± 0.00875	0.00016 ± 0.0006	1.0	0.0065 ± 0.0161	0.02716 ± 0.00075	4.3886 ± 0.1813	59.2 ± 2.4
1350	0.5872	4.4711 ± 0.0528	0.00339 ± 0.0101	0.0101 ± 0.00125	0	0.0062 ± 0.0185	0.02817 ± 0.00048	4.4434 ± 0.3718	59.9 ± 4.9
1500	0.5912	4.5876 ± 0.0732	-0.0139 ± 0.01703	-0.00102 ± 0.00136	-6.6	0.0255 ± 0.0313	0.02851 ± 0.00076	4.859 ± 0.4106	65.4 ± 5.4
2000	0.9118	4.4991 ± 0.0087	0.12091 ± 0.00062	0.00004 ± 0.00002	0.1	0.2219 ± 0.0011	0.02969 ± 0.00011	4.4674 ± 0.0108	60.2 ± 0.1
2500	0.9952	4.463 ± 0.0169	0.01025 ± 0.00079	0.00004 ± 0.00007	0.3	0.0188 ± 0.0015	0.02366 ± 0.00013	4.4231 ± 0.0263	59.6 ± 0.4
8500	1.0000	5.9917 ± 0.052	0.05306 ± 0.01125	0.00483 ± 0.00085	23.9	0.0974 ± 0.0207	0.0245 ± 0.0008	4.5389 ± 0.2546	61.2 ± 3.4
Integrated		4.5817 ± 0.0063	0.04191 ± 0.00029	0.00037 ± 0.00002	2.4	0.0769 ± 0.0005	0.02781 ± 0.00006	4.4456 ± 0.0091	59.9 ± 0.2

Note: The monitor mineral MMhb-1 (Samson and Alexander, 1987) with an age of 513.9 Ma (Lanphere and Dalrymple, 2000) was used to monitor neutron flux (and calculate the irradiation parameter, J). The samples and standards were wrapped in aluminum foil and loaded into aluminum cans of 2.5 cm diameter and 6 cm height. The samples were irradiated in position 5c of the uranium enriched research reactor of McMaster University in Hamilton, Ontario, Canada for 20 megawatt-hours. Upon their return from the reactor, the sample and monitors were loaded into 2-mm-diameter holes in a copper tray that was then loaded in an ultra-high vacuum extraction line. The monitors were fused, and samples heated, using a 6-watt argon-ion laser following the technique described in York et al. (1981), Layer et al. (1987), and Layer (2000). Argon purification was achieved using a liquid nitrogen cold trap and a SAES Zr-Al getter at 400 °C. The samples were analyzed in a VG-3600 mass spectrometer at the Geophysical Institute, University of Alaska Fairbanks. The argon isotopes measured were corrected for system blank and mass discrimination, as well as calcium, potassium and chlorine interference reactions following procedures outlined in McDougall and Harrison (1999). System blanks generally were 2 × 10<sup>-16</sup> mol <sup>40</sup>Ar and 2 × 10<sup>-16</sup> mol <sup>36</sup>Ar, which are 10 to 50 times smaller than fraction volumes. Mass discrimination was monitored by running both calibrated air shots and a zero-age glass sample. These measurements were made on a weekly to monthly basis to check for changes in mass discrimination.

<sup>#</sup>Radiogenic

<sup>†</sup>Weighted average of J from standards = 0.002451 ± 0.000009

<sup>‡</sup>Weighted average of J from standards = 0.002512 ± 0.000006

<sup>§</sup>Weighted average of J from standards = 0.007597 ± 0.000028

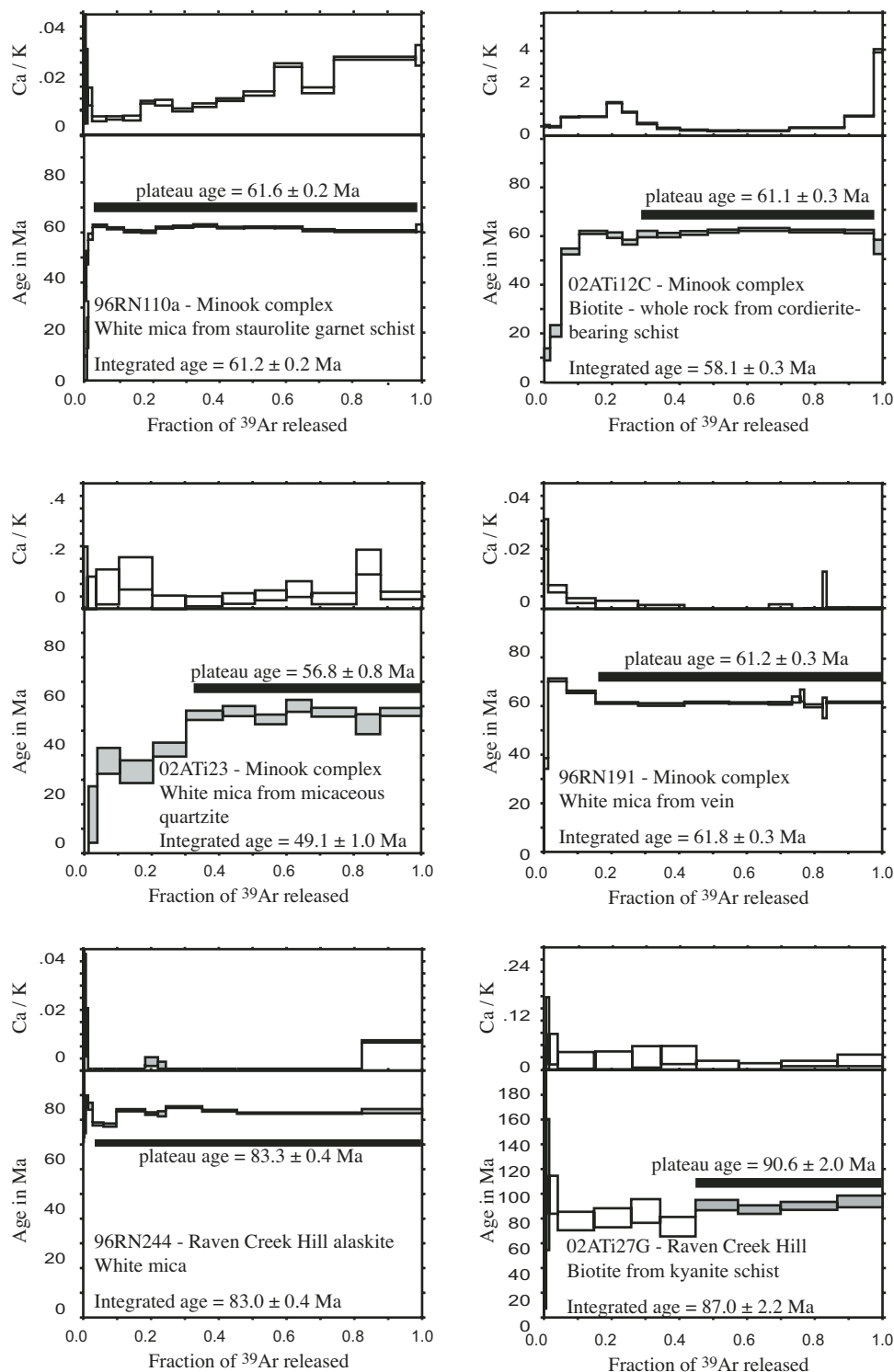


Figure 13. (continued on the next page)  $^{40}\text{Ar}/^{39}\text{Ar}$  spectra and Ca/K plots for metamorphic and igneous rocks, Rampart block and Manley pluton. Note that the scales used for both plots vary from sample to sample.

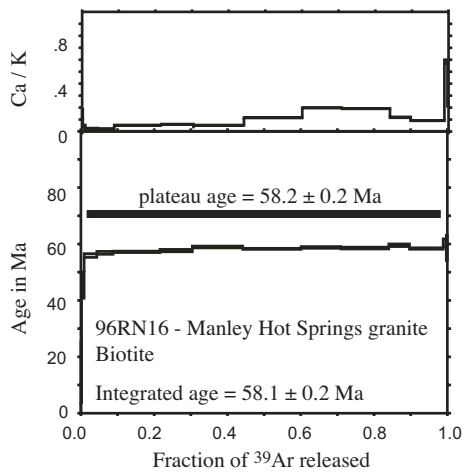
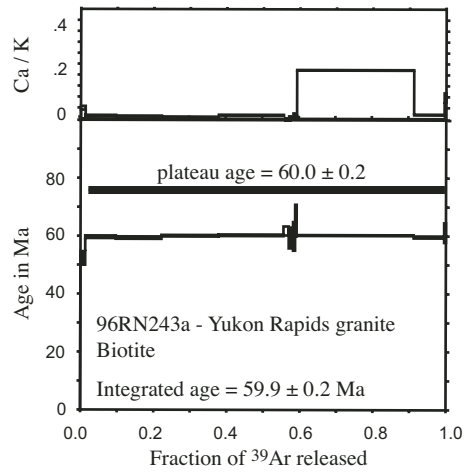
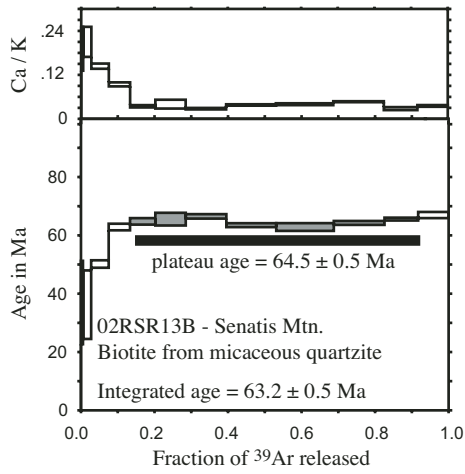
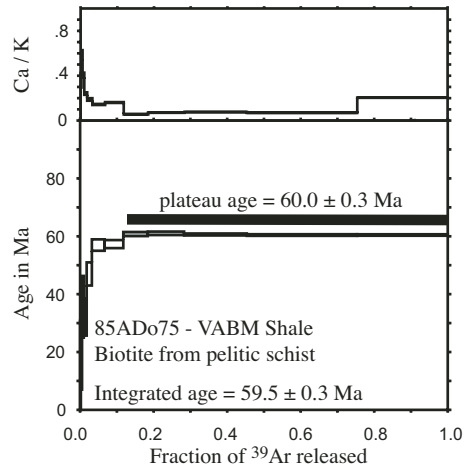
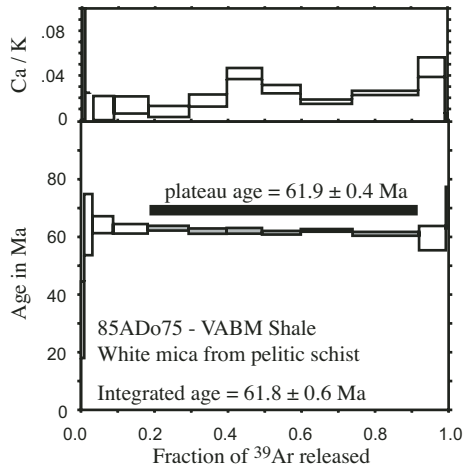
**Raven Creek Hill**

White mica from the alaskite body produced a plateau age of  $83.3 \pm 0.4$  Ma and an isochron age of  $82.5 \pm 0.5$  Ma (Fig. 14; sample 96RN244). A biotite age of  $90.6 \pm 2.0$  Ma was obtained from a kyanite-bearing schist (sample 02ATi27G). K-Ar ages of 66.5, 68, and 71.6 Ma from biotite schist have been reported (Chapman et al., 1971; Rinehart et al., 1997).

**VABM Shale**

$^{40}\text{Ar}/^{39}\text{Ar}$  ages obtained from fabric-forming white mica and biotite from two samples of pelitic schist yielded consistent plateau ages. White mica from sample 85ADo75B yielded an age of  $61.9 \pm 0.4$ . This is the sample that contained aligned andalusite. Biotite from that sample and a sample collected on an adjacent ridge yielded essentially identical plateau ages of  $60.0 \pm 0.3$  Ma.

Figure 13. (continued)



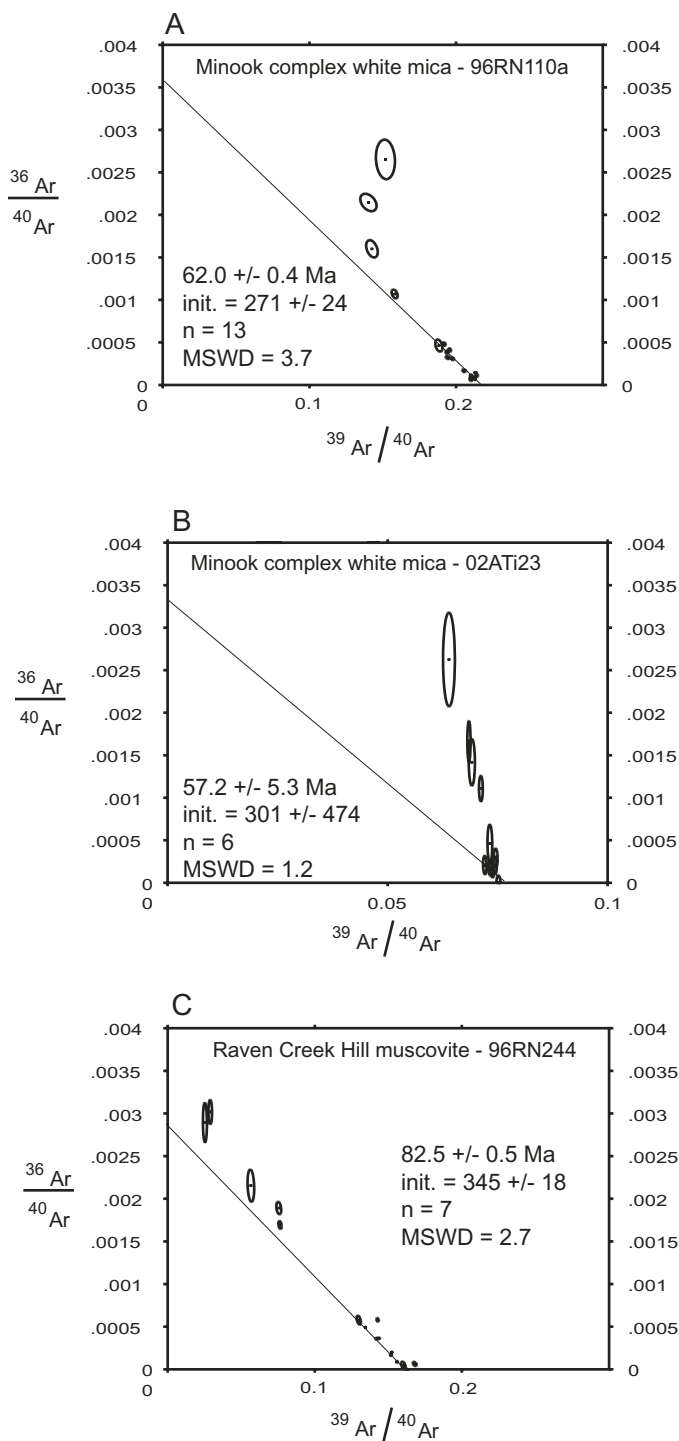


Figure 14. Inverse isochron plots, select  $^{40}\text{Ar}/^{39}\text{Ar}$  samples from the Minook complex and Raven Creek Hill.

### Senatis Mountain

Metaquartzite with a few percent mica (sample 02RSR13B) yielded a biotite plateau age of  $64.5 \pm 0.5$  Ma.

### Yukon Rapids Granite

Biotite from the granite yielded a plateau age of  $60.0 \pm 0.2$  Ma (sample 96RN243a). A K-Ar biotite analysis yielded essentially the same age,  $61.8 \pm 2.5$  Ma (Silberman et al., 1979).

### Manley Hot Springs Granite

Biotite from the granite yielded a plateau age of  $58.3 \pm 0.2$  Ma (sample 96RN16).

### Discussion of Geochronologic Data

Zircon ages from the Minook rhyolite, Yukon Rapids granite, and pegmatitic phase of Raven Creek Hill all overlap within error at 60 Ma. Micas cooled through the closure temperature for argon at ca. 60 Ma at several localities across the Rampart block, from the small metamorphic locality at VABM Shale to the Minook complex.

At the Minook complex,  $^{40}\text{Ar}/^{39}\text{Ar}$  plateau ages of micas from two of the schists (96RN110a; 02ATi12) and a cross-cutting vein (96RN191) overlap within error around 61 Ma. Results from sample 96RN110a, plotted on an inverse isochron diagram, show a simple array with an initial  $^{36}\text{Ar}/^{40}\text{Ar}$  ratio corresponding to the atmospheric value (Fig. 14A). This indicates, based on modeling assumptions, that there is no inherited (older) component of argon in the sample (McDougall and Harrison, 1999). The younger white mica plateau from sample 02ATi23 extends over less of the  $^{39}\text{Ar}$  release and has evidence of argon loss (see Fig. 13), which is not surprising considering the age of the crosscutting vein. The concordance of the date obtained from the cordierite-bearing schist (02ATi12C) with dates from staurolite-bearing schist and the gold-quartz vein indicates that the lower-pressure assemblages in the Minook complex cooled at the same time as the higher pressure (staurolite + kyanite) assemblages. Because the biotite-rich sample (02ATi12C) yielded the same plateau age as the white-mica-bearing samples, white mica and biotite passed through their respective closure temperatures essentially simultaneously at the Minook complex and the NW sliver, and 61 Ma is a minimum age for peak metamorphism of both packages.

At Raven Creek Hill, both argon and U-Pb isotope systematics are complex. Six monazites define the magmatic age for part of the alaskite at ca. 111 Ma, whereas clear pink zircons from the pegmatitic variant are concordant at ca. 60 Ma. Several monazites show Pb loss (Fig. 12), which was likely caused by the same event that produced the 60 Ma zircons. Field observations and available data are insufficient for us to determine whether the pegmatitic variant of the pluton was generated via in situ partial melting of a Cretaceous alaskite or whether it was somehow intimately injected into the older pluton. The mineralogy of the two phases of the alaskite is essentially the same; they do not appear to be

compositionally distinct. This is consistent with the coarser material having formed from in situ partial melting.

The spread in  $^{40}\text{Ar}/^{39}\text{Ar}$  and K-Ar ages from Raven Creek Hill (66–90 Ma), from the alaskite and the schists, is evidence that the argon system did not equilibrate there. The age spectrum and inverse isochron plot for the white mica collected from the pluton show a small but significant amount of inherited argon (96RN244, Fig. 14B), so it may be biased toward an old age. In light of the U-Pb isotope data, the 83 Ma age from the alaskite is difficult to interpret as geologically meaningful. Inverse isochron plots from the biotite schists did not show linear arrays. Micas in the metamorphic rocks may retain elements of both Cretaceous and Tertiary thermal events; the spread in the ages is consistent with this interpretation.

The geochronologic data available for the Minook complex and Raven Creek Hill do not allow direct comparison of their cooling histories. The fact that the Minook complex passed through white mica and biotite closure temperatures at 61 Ma whereas zircons crystallized in pegmatite at Raven Creek Hill at 60 Ma itself suggests their cooling histories might be different. Exhumation of the Minook complex was apparently under way while the Raven Creek Hill pegmatite was in the process of crystallizing.

Based on  $^{40}\text{Ar}/^{39}\text{Ar}$  data, rocks at VABM Shale cooled synchronously with those in the Minook complex. White mica from the metamorphic fabric that also contained aligned andalusite yielded a plateau age that overlaps within error white mica ages from the Minook complex; biotite ages are slightly younger than that from the biotite-rich whole rock separate from Minook. Cooling may have been slightly slower at VABM Shale than at Minook, although it is hard to estimate the likely closure temperature of a biotite-rich whole rock separate.

The older  $^{40}\text{Ar}/^{39}\text{Ar}$  age (64 Ma) obtained from a metaquartzite at Senatis Mountain is the most precise of several biotites analyzed from that sample, which yielded a variety of ages. This likely reflects intergrain scale intergrowth of chlorite, paragonite, an alteration phase in the original sample, or an inhomogeneously distributed component of argon inheritance. The Ca/K ratio of the lower temperature steps for the analysis is higher than the rest of the sample; correspondingly, apparent ages for those steps are lower than the plateau age. This pattern in Ca/K and lower T ages has been linked to mixed phases (e.g., Till and Snee, 1995) rather than argon loss.

Within the Rampart block, the overlap in zircon crystallization and argon cooling ages suggests rapid cooling. The Yukon Rapids granite cooled very quickly; the biotite age almost overlaps the zircon age within error ( $60.0 \pm 0.2$  and  $60.5 \pm 0.2$ ). Unfortunately, definition of a cooling history at Raven Creek Hill is not possible because of the unequilibrated  $^{40}\text{Ar}/^{39}\text{Ar}$  signal. However, similarities in the metamorphic assemblages and fabrics at Minook and Raven Creek Hill are consistent with their forming during the same event. The  $^{40}\text{Ar}/^{39}\text{Ar}$  cooling ages from the Minook complex are actually very slightly older than the zircon crystallization age for the alaskite at Raven Creek Hill.

In contrast, south of the Rampart block, the Manley Hot Springs granite cooled more slowly. The biotite age is slightly younger than the zircon crystallization age ( $60.9 \pm 1.0$  and  $58.7 \pm 0.2$ ). Based on the Yukon Rapids and Manley Hot Springs granites, cooling was more rapid within the Rampart block than outside the block.

## METAMORPHIC HISTORY

The petrogenetic grid presented in Figure 15 provides a qualitative framework for evaluating the P-T path(s) of Rampart block metamorphic rocks. Metamorphic paths are shown for the rocks of the Minook complex and Raven Creek Hill. Pelitic rocks in the two lenses preserve evidence of two prograde reactions. Garnets in two samples from the Minook complex contain chloritoid inclusions, indicating that the packages of rocks progressed across the reaction chloritoid = garnet + staurolite + biotite (Fig. 15, from area 1–2). Several samples contain the assemblage garnet-staurolite-biotite or kyanite-staurolite-biotite (Table 1; Fig. 7). Sample 02ATI24C equilibrated above the staurolite-out reaction because it contains the assemblage biotite-

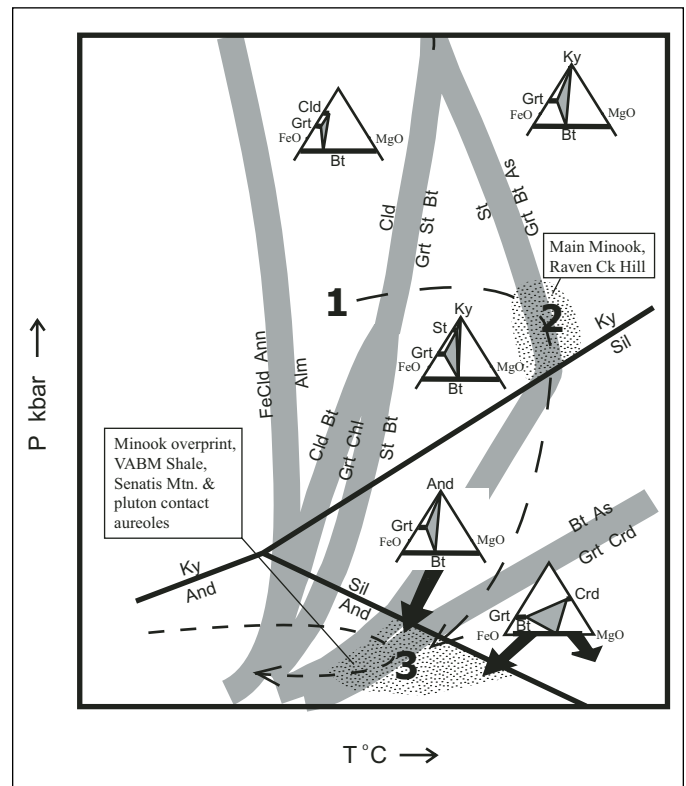


Figure 15. Pressure-temperature grid for pelitic rocks, modified from Spear and Cheney (1989) showing P-T conditions recorded in Rampart block metamorphic rocks. Numbers represent conditions determined from mineral assemblages. Dashed arrows represent two possible P-T paths for the Minook complex and Raven Creek Hill (see text for discussion).

garnet-kyanite and the garnets contain staurolite inclusions. This sample passed through the reaction (Fig. 7; in the presence of quartz, muscovite):

Staurolite = garnet + kyanite + biotite

This sample may have reached slightly higher temperature than the other samples or may have a bulk composition that triggers this reaction at lower temperatures than the other samples. Based on the assemblages in this and the other samples, peak metamorphic assemblages at the Minook complex and Raven Creek Hill crystallized at conditions near the terminal staurolite-out reaction. The intersection of the staurolite-out curve with the kyanite/sillimanite curve represents the minimum pressure and temperature conditions reached in the Minook complex.

The prograde metamorphic path of these rocks therefore passed through a chloritoid-stable field and culminated at conditions near the terminal staurolite-out reaction in the kyanite field for compositions represented by sample 02ATi24C (Fig. 15, area 2).

The metamorphic conditions recorded by (a) the one sample from the Minook complex with a secondary mineral assemblage of andalusite and biotite, (b) assemblages in the northwest sliver of the Minook complex, and (c) the northwest part of the Rampart block, at VABM Shale, Senatis Mountain, and the contact aureole of the Yukon Rapids pluton are all very similar. The conditions at which staurolite reacted to andalusite and biotite in sample 96KC56 are limited by the intersection of the staurolite-out curve with the andalusite-sillimanite curve. Pressures must have been lower and temperatures higher than the aluminosilicate triple point when the andalusite and biotite crystallized (Fig. 15, area 3). The assemblage cordierite plus garnet and biotite in the fine-grained pelitic rocks of the Minook complex NW sliver is stable at similar low-pressure, high-temperature conditions. The presence of andalusite and garnet at Senatis Mountain and of cordierite with gedrite in the contact aureole of the Yukon Rapids pluton indicates metamorphic conditions at low pressures and elevated temperatures for the northwest part of the Rampart block.

There are two possible interpretations of the metamorphic history recorded in the Rampart block, and they depend on the timing of the kyanite-producing metamorphic event (Fig. 15, area 2) relative to the lower-pressure event (Fig. 15, area 3). If the rocks of the Minook complex were at kyanite-stable conditions in the early Tertiary, the metamorphic path of the eastern Rampart block was a clockwise path that peaked near the staurolite-out reaction in the kyanite field, followed by significant decompression at elevated temperatures that resulted in crystallization of andalusite and biotite after staurolite. The thin sliver of graphitic metapelites on the NW side of the Minook complex was juxtaposed with the kyanite-bearing rocks during the exhumation phase of their metamorphic path, at approximately the same conditions recorded in the sample with andalusite after staurolite. Other metamorphic rocks in the central and western Rampart block—the contact zone of the Yukon Rapids pluton, Senatis Mountain, and VABM Shale—also record lower-pressure peak metamorphic conditions

than those at the Minook complex and Raven Creek Hill. In this scenario, the kyanite-bearing rocks were exhumed from significant depths adjacent to the Victoria Creek fault; away from the Victoria Creek fault, we see evidence of shallow metamorphism and deformation.

If the kyanite-stable event was significantly older than early Tertiary and rocks of the Minook complex and Raven Creek Hill were exhumed to relatively shallow depths prior to 60 Ma, then the overprint assemblage recorded in sample 96KC56 and the lower-pressure assemblages in the NW sliver of the Minook complex recorded a metamorphic overprint on the kyanite-bearing and adjacent, previously unmetamorphosed rocks, respectively. The P-T path for this scenario corresponds to the low-pressure isobaric loop that culminates in area 3 on Figure 15.

In either case, crustal processes resulted in exhumation of the more deeply metamorphosed rocks in slivers adjacent to the Victoria Creek fault, begging the question of the fault system's role in the exhumation process.

## STRUCTURAL CHARACTERISTICS

Macrostructures in rocks of the Rampart block include brittle fabrics in very-low-grade metabasites of the Tozitna terrane and penetrative, schistose fabrics that record progressive deformation in the Minook and Raven Creek Hill complexes. The contacts between rocks manifesting these two structural styles are not exposed but represent an abrupt change in P-T history and fabric intensity, and we consider them to be brittle faults. This interpretation is supported by apatite fission track data from the region that also require extensive post-60 Ma differential uplift of subblocks within the Rampart block (Till et al., 2004). As a consequence, we were unable to identify faults or shear zones that were active at 60 Ma and relate directly to the cooling history of the metamorphic complexes. No regional detachment is preserved, and thus, the current geometry is unlike a classic metamorphic core complex.

High-strain zones, defined by closely spaced planes and intense mineral lineations, are rare and well developed only in the contact aureole of the Yukon Rapids pluton. The section below summarizes observations of the macrostructures associated with ductile deformation in the Rampart block. All of these regions yield Ar/Ar cooling ages between 65 and 57 Ma with the exception of the Raven Creek Hill region (see geochronology discussion above).

In sum, the stretching direction in ductile fabrics from both shallow (andalusite-bearing) and deep (kyanite-bearing) metamorphic rocks in the Rampart block is NE-SW, subparallel to the Victoria Creek fault. This stretching direction is  $\sim 90^\circ$  from the regional NW-SE stretching direction in the Ruby terrane at the core of the Ruby geanticline, which records pre-Late Cretaceous fabrics (Dover, 1994; Roeske et al., 1995). The stretching direction is not well developed outside of the Rampart block. Contact zones of ca. 60 Ma plutons south of the Victoria Creek fault show little to no fabric development. Although stretching lineations with a similar NE orientation have been measured in the contact

aureole of the Manley pluton, they are very weak; none were seen in the contact aureole of the Tolovana pluton (Fig. 3).

**Yukon Rapids Pluton and Contact Aureole**

Foliations measured in the contact zone of the Yukon Rapids pluton dip gently to moderately to the SW (Fig. 16) and locally contain zones up to 20 cm wide showing grain-size reduction. We interpret these as ductile shear zones; S-C fabrics within them give a normal, down-to-the-southwest sense of slip. Mineral trains on all of the SW-dipping surfaces plunge moderately on average (47°), with close to a 90° pitch. Within 100 m of the pluton the fabric intensifies to an L-tectonite, also oriented 240–245° and plunging 10–20°. The high-T fabric in the pluton is defined by aligned hornblende and feldspar; these elongation directions show a greater scatter than the fabric in the pluton aureole, which may be due to a mixture of magmatic and submagmatic fabric elements.

All of the SW-trending mineral lineations from the contact aureole are interpreted to reflect elongation directions during pluton emplacement because they are subparallel to the map-scale elongation direction of the pluton and they are best developed in close proximity to the pluton.

Mineral lineations that trend to the northwest are from lower-grade, finer-grained rocks from a limited area north of the pluton. These outcrops may have been rotated during postmetamorphic faulting or may represent strain accumulated prior to intrusion of the pluton.

**Senatis Mountain**

Biotite-andalusite schists and micaceous metaquartzites on Senatis Mountain, the ridgeline immediately west of the Yukon Rapids pluton, display trains of biotite and muscovite and aligned andalusite trending WSW to SW, similar to those from the L-tectonite and ductile shear zones in the pluton aureole (Fig. 16).

**VABM Shale**

Lineations in the northernmost exposure of early Tertiary metamorphic rocks, near VABM Shale, are visible in most outcrops and oriented just a little east of north. These lineations are defined by trains of mica and aligned andalusite grains. In thin section fabrics prove to be variable, from those defined by well-aligned biotite, andalusite, and muscovite interlaminated with concentrations of fine-grained quartz to those with less intense laminations, late static growth of biotite, and plagioclase. The early Tertiary metamorphism around VABM Shale appears to have been accompanied by inhomogeneous deformation, and the macrostructures cannot be clearly related to the cooling ages.

**Minook and Raven Creek Hill**

Foliation in the Minook complex and Raven Creek Hill metamorphic rocks strikes from NNE to E and dips SE to NW. The range in foliation attitudes may be due to folding or faulting along

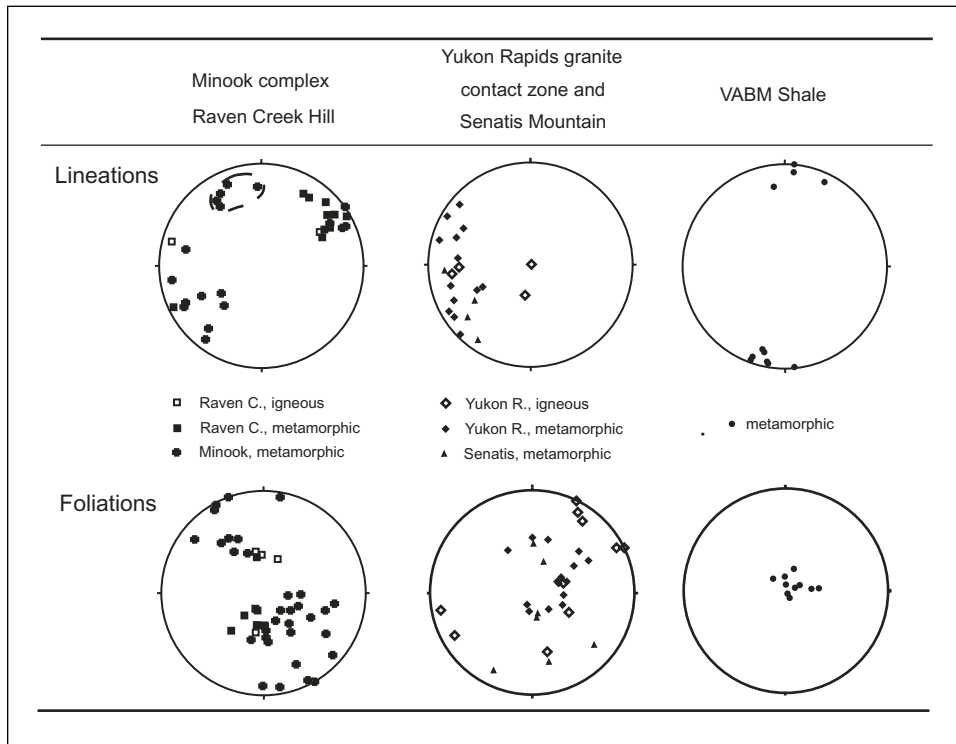


Figure 16. Equal-area lower hemisphere plots of foliation and lineation data from the Rampart block and Manley pluton contact zone. Dashed circles delineate measurements from small domains that might have been rotated by postmetamorphic brittle faults.

NE-SW-trending structures (Fig. 16). Elongation lineations, defined by mineral elongation (kyanite, staurolite) and mineral trains (garnet, staurolite), are dominantly oriented NE-SW. Rare tight folds of the foliation have hinge lines parallel to the mineral lineation. Tourmaline defines the mineral lineation in the pluton contact aureole at Raven Creek Hill; kyanite in the surrounding metamorphic rocks is aligned in the same NE direction. Although apatite fission-track data require the presence of a postmetamorphic fault between the schist/pluton contact and schist subcrops to the north at Raven Creek Hill (Till et al., 2004), the consistent NE-SW trend of mineral lineations suggests that postmetamorphic structures generally have not significantly rotated the Raven Creek Hill or Minook complex rocks. The one exception we can identify to this generalization is on the south side of the Minook complex. There, mineral lineations and pebble elongations measured in one set of outcrops yielded NNW-trending lineations (Fig. 16). These outcrops contain kyanite, so we believe this fabric was formed at the same time as others in the Minook complex but likely rotated along brittle structures during exhumation.

## TECTONIC EVOLUTION

Two important uncertainties in reconstruction of early Tertiary tectonic events in the Rampart block are the period of kyanite stability in the metamorphic rocks and the relative timing of exhumation in the Raven Creek Hill and Minook complexes. Specifically, if kyanite-bearing rocks were stable at 60 Ma at Raven Creek Hill *and* the Minook complex, then metamorphic assemblages and thermochronology indicate rapid exhumation of the metamorphic rocks through a large section of crust. If the metamorphic rocks were exhumed from kyanite-stable crustal settings before 60 Ma, the amount of early Tertiary exhumation was less. It is also possible that both sites saw the same prograde deformation-metamorphism path but that the Minook rocks moved upward through the crust prior to those at Raven Creek Hill. At 61–60 Ma, the Minook could have passed through muscovite closure temperatures while Raven Creek Hill still experienced relatively high P and T and zircons crystallized in the pegmatitic phase of the alaskite.

At Raven Creek Hill, mineral lineations in schist north of the pluton, in the pluton contact zone, and some within the pluton have the same trend, suggesting that all three exposures experienced deformation and recrystallization as a single package. The trend of tourmaline alignment in the contact zone is 061–63°, plunging 25–35°NE. Kyanite in the adjacent metamorphic rocks is oriented 052°, plunging 20°NE and 245°, plunging 5°SW (measured in outcrop and confirmed with oriented thin sections). These alignments are strikingly similar. The alaskite sample that yielded the clear pink 60 Ma zircons was collected in the contact zone, indicating the contact zone was hot during the early Tertiary, so rocks in the contact zone were capable of ductile deformation at that time. We believe that the tourmaline alignment formed during early Tertiary deformation. Because of the concordance of the tourmaline and

kyanite alignments and the needle shape of the kyanite grains in that alignment, we believe that the kyanite at Raven Creek Hill also was stable during early Tertiary deformation.

Alternatively, if we hypothesize that the alignment of the tourmaline and kyanite is a mid-Cretaceous phenomenon, we must consider the parallelism of that alignment with the mineral lineations in the contact aureole of the 60-Ma Yukon Rapids pluton purely coincidental. If we suppose that the kyanite is Cretaceous and the deformation responsible for its alignment is early Tertiary, the strongly elongate shape of the kyanite grains as they lie in the foliation and the lack of overprinting metamorphic assemblages must be explained. This is challenging considering that the presence of 60-Ma zircons in the contact zone of the alaskite pluton is evidence for an early Tertiary heat source near Raven Creek Hill in particular. However, we cannot show unequivocally that the kyanite was stable during the early Tertiary; the kyanite-bearing metamorphic rocks could have been at shallower levels of the crust by that time. Even if they were at shallower levels, a tectonic model for the history of the Rampart block must still feature exhumation of rocks exhibiting the deepest crustal histories adjacent to the Victoria Creek fault—but at an unknown rate.

The discussion below is predicated on our belief that the kyanite-bearing peak metamorphic assemblages in the Minook complex and Raven Creek Hill were stable during the earliest Tertiary.

## Metamorphic Exhumation Paths and Strike-Slip Faulting

Ductile fabrics developed in metamorphic culminations and associated plutons of the Rampart block show a pattern of generally northeast-southwest elongation parallel to the southern boundary of the block, the Victoria Creek fault. Some of these fabrics formed at relatively high-P conditions, as documented by staurolite- and kyanite-bearing mineral lineations in metamorphic rocks in the Minook complex and at Raven Creek Hill, adjacent to the fault. The same orientations are documented in the alaskite pluton associated with kyanite schist at Raven Creek Hill and in the shallower contact aureoles and ductile shear zones immediately adjacent to early Tertiary plutons. As summarized below, the combination of all of these data indicates the whole region underwent strain that was associated with slip on the Victoria Creek fault.

Because the mineral lineations in the highest-strain rocks are consistently oriented subparallel to one another and both the high-P and low-P fabrics appear to have formed in one progressive deformation event, we interpret the mineral lineations as recorders of the finite strain maximum stretch direction during the early Tertiary and not as the result of overprinting finite strain from unrelated events. The subparallel nature of these fabrics to the Victoria Creek Fault and the focusing of exhumation along it clearly link the exhumation process to either transpression or transtension. Orogen-parallel stretching lineations can develop in both transpression and transtension (Dewey et al., 1998; Fossen and Tikoff, 1998), depending on the ratios of the coaxial components, i.e., whether the deformation zone is undergoing overall

stretching or shortening in the x, y, and z directions. Net extension can occur during transpression where the zone of deformation is not laterally confined (e.g., Avé Lallemant and Guth, 1990; Jones et al., 1997). However, transpressional scenarios do not account for simultaneous bimodal volcanism and ductile deformation, whereas transtensional deformation accounts for all of the observed geologic features. Net extension subperpendicular to the Victoria Creek fault accounts for widespread bimodal volcanism, synchronous localization of subsidence (basins) and uplift (exhumation) along strike-slip strands and indicates a complex partitioning of vertical motion within the overall broad field of transtension. The remaining question, why transtension was focused in this particular part of Alaska, is addressed in the section below.

### Early Tertiary Tectonic Processes

The Rampart block sat in a broad regional zone of within-plate magmatism during the early Tertiary. Bimodal volcanic and plutonic rocks are exposed north of the Tintina fault system on both flanks of the Ruby geanticline and south of the Tintina fault system in the Yukon Tanana Upland (Fig. 2).  $^{40}\text{Ar}/^{39}\text{Ar}$  and most K-Ar ages from bimodal intrusives in the Yukon-Tanana Upland range from 55 to 61 Ma (Newberry, 2000). Biotite monzonite and syenogranite are typical of the more felsic magmas; diabase dikes and sills are typical of the more basaltic. Trace element concentrations suggest a within-plate origin for these rocks (Newberry, 2000; Fig. 4). These rocks could have formed as a result of shallow subduction or passage of a slab window, which has been well documented during this time frame in the southern Alaska accretionary prism (Bradley et al., 2003; Sisson et al., 2003).

Basins of Late Cretaceous and early Tertiary age occur along the Tintina fault system. North of the fault system, the Yukon Flats basin is underlain by a thick sequence of unknown, but likely pre-Miocene, age. The deepest part of the basin contains more than 8500 m of material, based on interpretation of gravity data (Morin et al., 2005; Phillips and Saltus, 2005), and sits immediately north of the Tintina fault system (Fig. 2). The uppermost, regionally extensive units in the Yukon Flats basin stratigraphy are generally undeformed and probably Miocene (Till et al., 2005). Late Cretaceous, Paleocene, and Eocene strata are exposed along the Tintina system southeast and southwest of the Yukon Flats basin (Figs. 2, 3). In the Rampart block, sedimentary rocks record a transition from deposition in through-going fluvial basins to more restricted fluvial and lacustrine basins at the Cretaceous/Tertiary boundary (Farmer et al., 2003).

Basin development was synchronous with bimodal magmatism and metamorphism in the Rampart block. The concentration of crustal deformation within the Rampart block adjacent to the Victoria Creek fault remains to be explained. Three scenarios can be outlined: coincidence of high heat flow with a local stepover within the Tintina fault system; coincidence of high heat flow with a stepover at a very large scale, linking movement on the Tintina and Kobuk fault systems; and coinci-

dence of high heat flow with oroclinal bending. Figure 17 summarizes the timing of features related to these scenarios, which are shown in Figure 18.

### Local-Scale Steptover

The Rampart block sits between the Tozitna and Victoria Creek faults. Though the early Tertiary spatial relationship of the faults isn't known, the long-term sense of motion on the Tintina system, which includes the Victoria Creek fault, is right-lateral; motion on the Tozitna fault appears to be right-lateral (Dover, 1994). The unique presence of early Tertiary metamorphism and ductile deformation between these fault strands may have been produced in a releasing stepover (Fig. 18A). This setting is analogous to that described by Monastero et al. (2005) for metamorphism and deformation at the Coso geothermal field, SE California. The interaction of thermally softened lithosphere and strike-slip tectonics there has resulted in a concentration of crustal thinning between faults in a releasing stepover at a scale similar to early Tertiary deformation in the Rampart block. However, this scenario would predict that the extension direction in the metamorphic complexes and the elongation direction of the plutons would be oblique to the main dextral slip fault, rather than the parallel orientation we observed.

### Regional-Scale Steptover

The Yukon Flats basin sits between the right-lateral Kobuk and Tintina fault systems in the position of a releasing stepover on a much larger scale than described above. The basin is younger

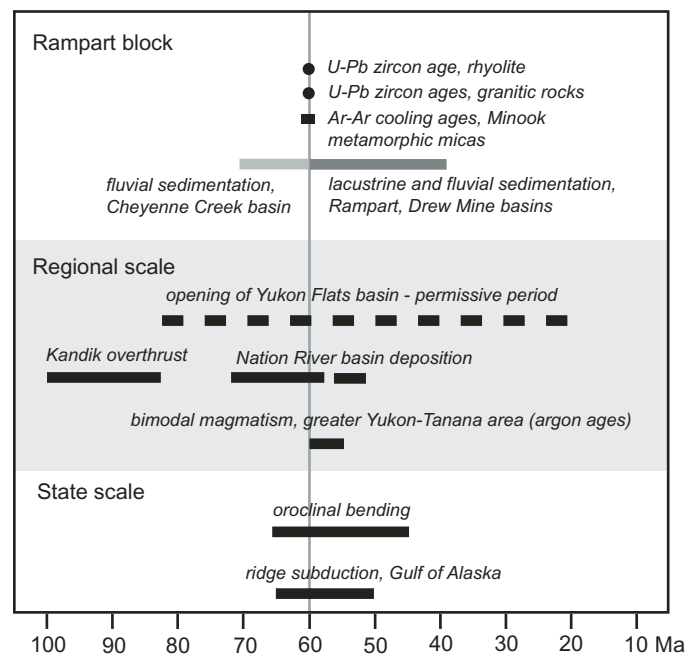


Figure 17. Plot of geologic events versus time at local, regional, and state scales pertinent to the tectonic evolution of the Rampart block.

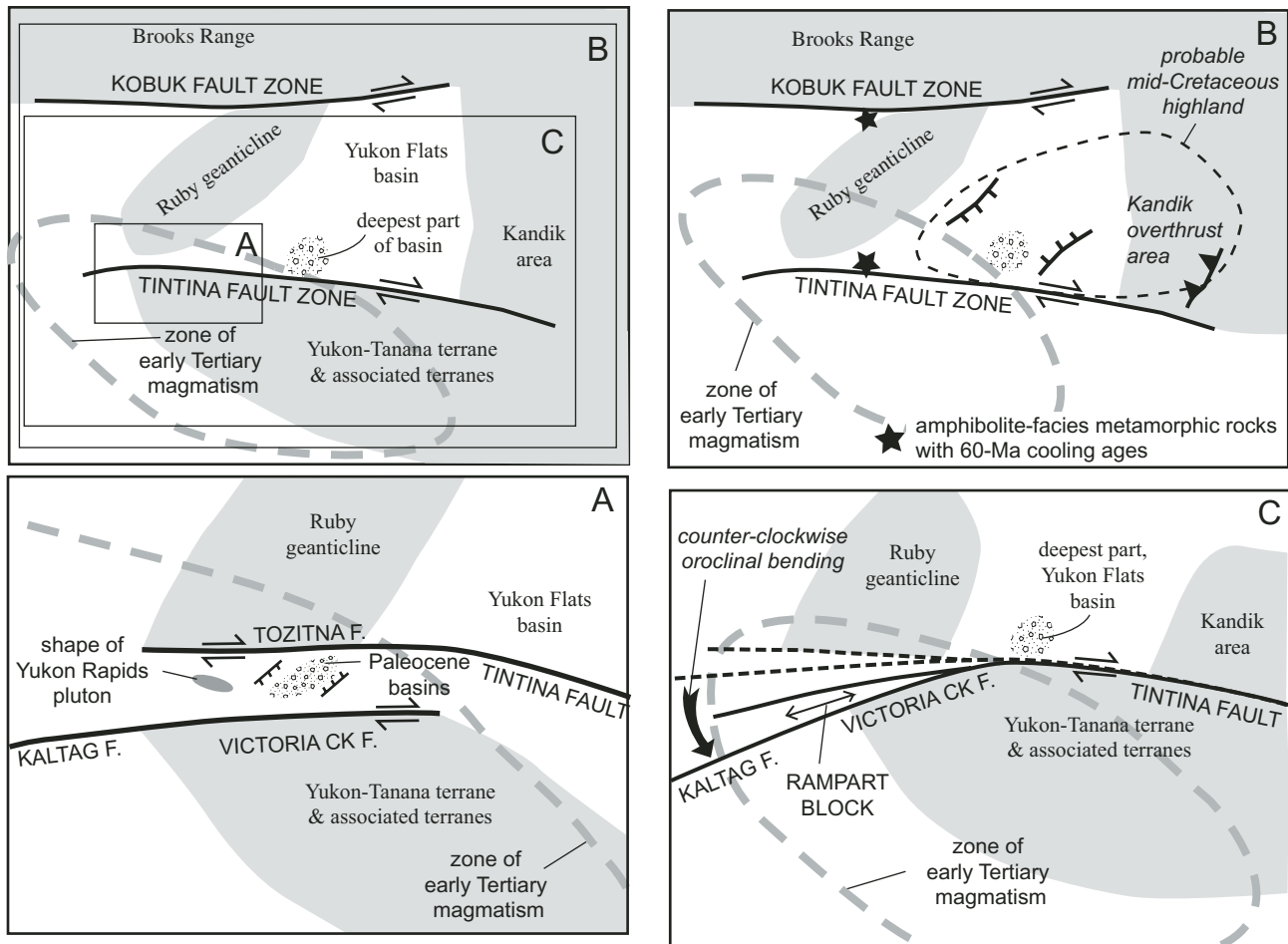


Figure 18. Possible tectonic scenarios for generation of relationships documented in the Rampart block and associated rocks during the early Tertiary. Relative location of panels A, B, and C is shown in the first panel.

than Albian, based on relationships in the Kandik area, on the southeast basin margin (Fig. 2). There, a sequence of Jurassic and Lower Cretaceous deep-water strata was thrust eastward over the North American margin in Cenomanian to Campanian time, based on apatite fission track data collected across the major frontal thrust (Underwood et al., 1996). During the thrusting event, the area now occupied by the Yukon Flats basin must have been a topographic high to mechanically support thrusting to the east. The Maastrichtian to Eocene(?) Nation River basin sits atop this thrust belt (Fig. 2). The Nation River basin is interpreted to be an extensional basin localized along former thrust faults that were reactivated as extensional faults by movement on the Tintina fault system (Van Kooten et al., 1997; Johnsson, 2000). The extensive Yukon Flats basin may have been nucleated at the same time as the Nation River basin by movement on the Tintina and Kobuk fault systems. In this scenario, concentration of deformation and metamorphism in the Rampart block during the early Tertiary might have resulted from spatial overlap of the southern boundary of the Kobuk-Tintina stepover with high thermal gradients associated with magmatism (Fig. 18B). Although this sce-

nario accounts for development of the Yukon Flats basin, it doesn't explicitly show how deformation was focused in the Rampart block.

#### Oroclinal Bending

Based on paleomagnetic evidence, the southern Alaska orocline is thought to have formed by a  $44 \pm 11^\circ$  counterclockwise rotation of western Alaska sometime between 66 and 44 Ma (e.g., Hillhouse and Coe, 1994). How much oroclinal bending happened before, during, and after 60 Ma is unknown. If oroclinal bending was under way at 60 Ma, an increase in curvature of the Tintina fault system could have caused transtension in the Rampart block and areas along the fault system (Fig. 18C). The deepest part of the Yukon Flats basin is along its southern margin, adjacent to the Tintina fault system (Fig. 2). The Nation River basin could mark the eastern end of the transtensional zone. The unique presence of early Tertiary metamorphic rocks in the Rampart block may be due to the coincidence of this transtensional zone with an area of high heat flow during the early Tertiary magmatic event. This scenario requires that rocks on the south side of

the Tintina fault zone reacted more rigidly to oroclinal bending than those on the north side during the early Tertiary.

The tectonic scenarios described above are not mutually exclusive and may have operated in concert to produce observed relationships. However, none of these scenarios account well for the focus of deformation and for the apparently uneven magnitude of exhumation within the Rampart block. In particular, the presence of the kyanite-bearing rocks of the Minook complex and Raven Creek Hill adjacent to the Victoria Creek fault requires that exhumation processes operated with greater efficiency near the fault. We have no specific model to explain this relationship but believe it may be an important and unusual example of exhumation in strike-slip systems worthy of further study.

Other early Tertiary (Paleocene) metamorphic complexes occur adjacent to strike-slip faults in Alaska, suggesting a coincidence between crustal heating, strike-slip faulting, and uplift in several parts of the state. Roeske et al. (2003) described amphibolite-facies metasedimentary and metaigneous rocks with strong ductile fabrics along the Kobuk fault zone, 200 km north of the Rampart block (Figs. 1, 18B). The geometry of the ductile fabrics and cooling ages from the schists are consistent with early Tertiary exhumation of the amphibolite-facies rocks in a dextral-slip fault system. In southern Alaska, Paleocene greenschist-facies metapelitic rocks are exposed immediately north of the Castle Mountain fault (Fig. 1; Harlan et al., 2003), a dextral-slip fault active in the forearc in the early Tertiary (Grantz, 1966; Bunds, 2001). The metamorphic rocks also sit structurally below remnants of a Paleocene nonmarine sedimentary and volcanic sequence (Trop et al., 2003). The structural juxtaposition of metamorphic rocks cooled in the early Tertiary with the overlying unmetamorphosed early Tertiary clastic sedimentary rocks suggests that a detachment adjacent to the Castle Mountain fault was an important early Tertiary structure. The Castle Mountain, Rampart, and Kobuk early Tertiary metamorphic complexes line up along the hinge of the Alaska orocline. All of these complexes may be related to some combination of high heat flux, strike-slip motion, and oroclinal bending.

In the Rampart block, final emplacement of the kyanite schists at the surface was accomplished by multiple pulses of brittle faulting in the upper crust later in the Tertiary. Apatite fission track analyses indicate that the Minook complex and Raven Creek Hill moved within 4 km of the paleosurface in pulses at ca. 44 Ma, ca. 36 Ma, and around ca. 26 Ma (Till et al., 2004). The Victoria Creek fault was active during the youngest pulse of deformation along the fault, at ca. 23 Ma, and likely was active throughout.

## CONCLUSIONS

Rocks of the Rampart block record coeval basin formation, bimodal volcanism, ductile deformation, and metamorphic cooling during the early Tertiary. The coincidence of basin formation with bimodal volcanism and the nature of ductile deformation features suggests that the Rampart block was a zone of transtension likely related to movement on the Victoria Creek fault, a major splay of the Tintina strike-slip fault system. Exposures of

kyanite grade metamorphic rocks in the Rampart block adjacent to the Victoria Creek fault are evidence that exhumation was greatest near the strike-slip system; deeply metamorphosed rocks with early Tertiary cooling ages are nowhere else exposed in areas flanking the Tintina fault system in central Alaska. The major structures that operated during the early Tertiary were overprinted by younger Tertiary brittle deformation along the Victoria Creek fault, and their nature remains obscure.

## ACKNOWLEDGMENTS

We are indebted to Rocky Riefenstahl, Rainer Newberry, and other geologists with the Alaska Division of Geological and Geophysical Surveys, whose detailed mapping and geochronologic studies first brought our attention to the complexity of early Tertiary evolution of the Rampart area and who loaned us thin sections. Many thanks to Brian Joy for exacting thin section aluminosilicate identification. We thank USGS reviewers Andrew Calvert and Karl Kellogg for their thoughtful insights. Comments from Jim Sample and two anonymous reviewers resulted in significant changes and improvements.

## APPENDIX. U-Pb ANALYTICAL TECHNIQUES

Zircon and other accessory phases were separated from samples using conventional crushing, grinding, and wilfley table techniques, followed by final concentration using heavy liquids and magnetic separations. Mineral fractions for analysis were selected based on grain quality, size, magnetic susceptibility, and morphology. All zircon fractions were air abraded prior to dissolution to minimize the effects of surface-correlated Pb-loss, using the technique of Krogh (1982). They were then washed with warm ultrapure 3N HNO<sub>3</sub>, (monazites washed with 1 N HNO<sub>3</sub>), rinsed with ultrapure water and subboiled acetone and weighed (to ±2μg). Zircons were dissolved in 300 μL PTFE or PFA microcapsules with ~100 μL of sub-boiled 29N HF and ~15 μL of sub-boiled 14N HNO<sub>3</sub> in the presence of a mixed <sup>233-235</sup>U-<sup>205</sup>Pb tracer for 40 hours at 240°C. Dissolution took place in stainless steel Parr bombs with 250 mL Teflon PTFE liners. Sample solutions were then dried to salts at ~125 °C and rebombed in ultrapure ~200 μL 3.1N HCl for 12 hours at 210 °C. Monazites were dissolved in ~1 mL of subboiled 6.2 N HCl for a minimum of 72 hours in 3.5 ml PFA screw top beakers on a hot plate at ~125 °C, also in the presence of a mixed <sup>233-235</sup>U-<sup>205</sup>Pb tracer. These solutions were then dried to salts on a hot plate at ~125 °C and redissolved in ~0.5 mL 3.1 HCl on a hot plate at ~125 °C. Pb and U separation for both zircon and monazite employed ion exchange column techniques similar to those described by Parrish et al. (1987). Pb and U were eluted sequentially into the same beaker followed by the addition of ~10 μL of 0.6N ultra pure phosphoric acid. Each sample was loaded onto a single zone refined Re filament using a phosphoric acid-silica gel emitter (SiCl<sub>4</sub>). Isotopic ratios were measured using a modified single collector VG-54R thermal ionization mass spectrometer equipped with an analogue Daly photomultiplier. Both U and Pb, respectively, were run at 1450 °C

in peak-switching mode on the Daly detector. U fractionation was determined directly on individual runs using the  $^{233-235}\text{U}$  tracer, and Pb isotopic ratios were corrected for fractionation of 0.37%/amu, based on replicate analyses of the NBS-981 Pb standard and the values recommended by Thirlwall (2000). U analytical blanks were less than 1 pg and Pb less than 3 pg. Common Pb isotopic compositions are derived from the model of Stacey and Kramers (1975). All analytical errors were numerically propagated through the entire age calculation using the technique of Roddick (1987). Analytical data are reported in Table 3. Concordia intercept ages and associated errors were calculated using a modified version the York-II regression model (wherein the York-II errors are multiplied by the MSWD) and the algorithm of Ludwig (1980). All ages are quoted at the 2 sigma level of uncertainty.

## REFERENCES CITED

- Avé Lallemant, H.G., and Guth, L.R., 1990, Role of extensional tectonics in exhumation of eclogites and blueschists in an oblique subduction setting, northeast Venezuela: *Geology*, v. 18, p. 950–953, doi: 10.1130/0091-7613(1990)018<0950:ROETIE>2.3.CO;2.
- Barker, J.C., 1986, Placer gold deposits of the Eagle trough, upper Yukon River region, Alaska: U.S. Bureau of Mines Information Circular 9123, p. 20.
- Beaudoin, B.C., Fuis, G.S., Lutter, W.J., Mooney, W.D., and Moore, T.E., 1994, Crustal velocity structure of the northern Yukon-Tanana Upland, central Alaska: Results from TACT refraction/wide-angle reflection data: *Geological Society of America Bulletin*, v. 106, no. 8, p. 981–1001, doi: 10.1130/0016-7606(1994)106<0981:CVSOTN>2.3.CO;2.
- Bradley, D., Kusky, T., Haeussler, P., Goldfarb, R., Miller, M., Dumoulin, J., Nelson, S., and Karl, S., 2003, Geologic signature of early Tertiary ridge subduction in Alaska, *in* Sisson, V.B., Roeske, S., and Pavlis, T.L., eds., *Geology of a Transpressional Orogen Developed during Ridge-Trench Interaction along the North Pacific Margin*: Geological Society of America Special Paper 371, p. 19–49.
- Bradley, D.C., Wooden, J., McClelland, W., Till, A., Roeske, S., and Miller, M.L., 2004, Detrital zircon geochronology of problematic terranes in interior Alaska: Alaska Geological Society 2004 Technical Conference, Abstracts, p. 11.
- Brosigé, W.P., Lanphere, M.A., Reiser, H.N., and Chapman, R.M., 1969, Probable Permian age of the Rampart Group, central Alaska: U.S. Geological Survey Professional Paper 1294-B, p. B1–B18.
- Bunds, M.P., 2001, Fault strength and transpressional tectonics along the Castle Mountain strike-slip fault, southern Alaska: *Geological Society of America Bulletin*, v. 113, no. 7, p. 908–919, doi: 10.1130/0016-7606(2001)113<0908:FSATTA>2.0.CO;2.
- Chapman, R.M., Weber, F.R., and Taber, B., 1971, Preliminary geologic map of the Livengood quadrangle, Alaska: U.S. Geological Survey Open-File Report 71-66, scale 1:250,000, 2 plates.
- Cushing, G.W., Meisling, K.E., Christopher, R.A., and Carr, T.R., 1986, The Cretaceous and Tertiary evolution of the Tintina fault zone, east-central Alaska: *Geological Society of America Abstracts with Programs*, v. 18, no. 2, p. 98.
- Dewey, J.F., Holdsworth, R.E., and Strachan, R.A., 1998, Transpression and transtension zones, *in* Holdsworth, R.E., Strachan, R.A., and Dewey, J.F., eds., *Continental Transpressional and Transtensional Tectonics*: Geological Society [London] Special Publication 135, p. 1–14.
- Dover, J.H., 1994, Geology of part of east-central Alaska, *in* Plafker, B., and Berg, H.C., eds., *The Geology of Alaska*: Geological Society of America, *Geology of North America*, v. G-1, p. 153–204.
- Dusel-Bacon, C., Brosigé, W.P., Till, A.B., Doyle, E.O., Mayfield, C.F., Reiser, H.N., and Miller, T.P., 1989, Distribution, facies, ages, and proposed tectonic association of regionally metamorphosed rocks in northern Alaska: U.S. Geological Survey Professional Paper 1497-A, 44 p.
- Dusel-Bacon, C., Lanphere, M.A., Sharp, W.D., Layer, P.W., and Hansen, V.L., 2002, Mesozoic thermal history and timing of structural events for the Yukon-Tanana Upland, east-central Alaska— $^{40}\text{Ar}/^{39}\text{Ar}$  data from metamorphic and plutonic rocks: *Canadian Journal of Earth Sciences*, v. 39, no. 6, p. 1013–1051, doi: 10.1139/e02-018.
- Farmer, E.T., 2004, Sedimentary basin development along major strike-slip fault systems: Tintina-Kaltag fault system of Alaska and the North Anatolian fault system of Turkey [M.S. thesis]: West Lafayette, Indiana, Purdue University, 186 p.
- Farmer, E.T., Ridgway, K.D., Bradley, D.C., and Till, A.B., 2003, Cretaceous-Early Eocene two-stage basin development, Yukon Flats basin, north-central Alaska: *Geological Society of America Abstracts with Programs*, v. 35, no. 6, p. 560.
- Fossen, H., and Tikoff, B., 1998, Extended models of transpression and transtension, and application to tectonic settings, *in* Holdsworth, R.E., Strachan, R.A., and Dewey, J.F., eds., *Continental Transpressional and Transtensional Tectonics*: Geological Society Special Publication 135, p. 15–33.
- Gabrielse, H., 1985, Major dextral transcurrent displacements along the Northern Rocky Mountain Trench and related lineaments in north-central British Columbia: *Geological Society of America Bulletin*, v. 96, no. 1, p. 1–14, doi: 10.1130/0016-7606(1985)96<1:MDTDAT>2.0.CO;2.
- Grantz, A., 1966, Strike-slip faults in Alaska: U.S. Geological Survey Open-File Report 66-53, 82 p.
- Hansen, V.L., and Dusel-Bacon, C., 1998, Structural and kinematic evolution of the Yukon-Tanana upland tectonites, east-central Alaska: A record of late Paleozoic to Mesozoic crustal assembly: *Geological Society of America Bulletin*, v. 110, p. 211–230, doi: 10.1130/0016-7606(1998)110<0211:SAKEOT>2.3.CO;2.
- Harlan, S.S., Snee, L.W., Vielreicher, R.M., Goldfarb, R.G., Mortensen, J., and Bradley, D.C., 2003, Age and cooling history of gold deposits and host rocks in the Willow Creek mining district, Talkeetna Mountains, south-central Alaska: *Geological Society of America Abstracts with Programs*, v. 36, no. 5, p. 235.
- Hillhouse, J.W., and Coe, R.S., 1994, Paleomagnetic data from Alaska, *in* Plafker, G., and Berg, H.C., eds., *The Geology of Alaska*: Geological Society of America, *Geology of North America*, v. G-1, p. 797–812.
- Jackson, L.E., Jr., and Mortensen, J.K., 2000, New constraints indicate mainly early Paleogene displacement on the Tintina fault zone in the northern Cordillera: *Geological Society of America Abstracts with Programs*, v. 32, no. 6, p. 21.
- Johnsson, M.J., 2000, Tectonic assembly of east-central Alaska: Evidence from Cretaceous-Tertiary sandstones of the Kandik River terrane: *Geological Society of America Bulletin*, v. 112, no. 7, p. 1023–1042, doi: 10.1130/0016-7606(2000)112<1023:TAOECA>2.3.CO;2.
- Jones, R.R., Holdsworth, R.E., and Bailey, W., 1997, Lateral extrusion in transpression zones: The importance of boundary conditions: *Journal of Structural Geology*, v. 19, no. 9, p. 1201–1207, doi: 10.1016/S0191-8141(97)00034-5.
- Kretz, R., 1983, Symbols for rock-forming minerals: *The American Mineralogist*, v. 68, p. 277–279.
- Krogh, T.E., 1982, Improved accuracy of U-Pb zircon ages by the creation of more concordant systems using an air abrasion technique: *Geochimica et Cosmochimica Acta*, v. 46, p. 637–649, doi: 10.1016/0016-7037(82)90165-X.
- Lanphere, M.A., and Dalrymple, G.B., 2000, First-principles calibration of  $^{38}\text{Ar}$  tracers: Implications for the ages of  $^{40}\text{Ar}/^{39}\text{Ar}$  fluence monitors: U.S. Geological Survey Professional Paper 1621, 10 p.
- Layer, P.W., 2000,  $^{40}\text{Ar}/^{39}\text{Ar}$  age of the El'gygytgyn impact event, Chukotka, Russia: *Meteoritics & Planetary Science*, vol. 35, no. 3, pp. 591–599.
- Layer, P.W., Hall, C.M., and York, D., 1987, The derivation of  $^{40}\text{Ar}/^{39}\text{Ar}$  age spectra of single grains of hornblende and biotite by laser step heating: *Geophysical Research Letters*, v. 14, p. 757–760.
- Ludwig, K.R., 1980, Calculation of uncertainties of U-Pb isotopic data: *Earth and Planetary Science Letters*, v. 46, p. 212–220, doi: 10.1016/0012-821X(80)90007-2.

- McDougall, I., and Harrison, T.M., 1999, *Geochronology and Thermochronology by the  $^{40}\text{Ar}/^{39}\text{Ar}$  Method*, 2nd ed.: New York, Oxford University Press, 269 p.
- Monastero, F.C., Katzenstein, A.M., Miller, J.S., Unruh, J.R., Adams, M.C., and Richards-Dinger, K., 2005, The Coso geothermal field: A nascent metamorphic core complex: *Geological Society of America Bulletin*, v. 117, no. 11/12, p. 1534–1553, doi: 10.1130/B25600.1.
- Morin, R.L., Stanley, R.G., Kumar, N., and Taylor, D.J., 2005, Geophysical expression of the Yukon Flats basin, east-central Alaska: *Geological Society of America Abstracts with Programs*, v. 37, no. 4, p. 94.
- Mortensen, J.K., and Von Gaza, P., 1992, Application of Landsat TM thermal imagery to structural interpretations of the Tintina Trench in west-central Yukon Territory: *Yukon Geology*, Report 3, p. 214–223.
- Newberry, R.J., 2000, Mineral deposits and associated Mesozoic and Tertiary igneous rocks within interior Alaska and adjacent Yukon portions of the 'Tintina gold belt': A progress report, in Tucker, T.L., and Smith, M.T., session chairs, *The Tintina Gold Belt: Concepts, Exploration, and Discoveries: Vancouver, British Columbia, British Columbia and Yukon Chamber of Mines Special Volume 2*, p. 59–88.
- Newberry, R.J., and Haug, S.A., 1997, CIPW norm, trace element, and Sr isotopic data for igneous rocks of the Tanana B-1 quadrangle and vicinity: Alaska Division of Geological and Geophysical Surveys Public Data File 97-293, 15 p.
- Parrish, R., Roddick, J.C., Loveridge, W.D., and Sullivan, R.W., 1987, Uranium-lead analytical techniques at the geochronology laboratory, Geological Survey of Canada, in *Radiogenic Age and Isotopic Studies*, Report 1, Geological Survey of Canada, Paper 87-2, p. 3–7.
- Patton, W.W., Jr., Box, S.E., Moll-Stalcup, E.J., and Miller, T.P., 1994, Geology of west-central Alaska, in Plafker, B., and Berg, H.C., eds., *The Geology of Alaska: Geological Society of America, Geology of North America*, v. G-1, p. 241–269.
- Phillips, J.D., and Saltus, R.W., 2005, Thickness of sedimentary rocks in the Yukon Flats basin, east-central Alaska, as estimated using constrained iterative gravity inversion: *Geological Society of America Abstracts with Programs*, v. 37, no. 4, p. 94.
- Reifenstuhel, R., Dover, J.H., Newberry, R.J., Clautice, K.H., Liss, S.A., Blodgett, R.B., Bundtzen, T.K., and Weber, F.W., 1997a, Interpretive geologic bedrock map of the Tanana B-1 quadrangle, central Alaska: Alaska Division of Geological and Geophysical Surveys Report of Investigations 97-15b, 1:63,360, 1 sheet, 15 p.
- Riefenstuhel, R.R., Layer, P.W., and Newberry, R.J., 1997b, Geochronology ( $^{40}\text{Ar}/^{39}\text{Ar}$ ) of 17 Rampart-area rocks, Tanana and Livengood quadrangles, central Alaska: Alaska Division of Geological and Geophysical Surveys Public Data File 97-29H, 21 p.
- Rinehart, C.D., Light, T.D., and Shew, N.B., 1997, Petrography and radiometric ages for selected rocks from the Livengood quadrangle, Alaska: U.S. Geological Survey Open-File Report 97-484D, 22 p.
- Roddick, J.A., 1967, Tintina Trench: *The Journal of Geology*, v. 75, p. 23–32.
- Roddick, J.C., 1987, Generalized numerical error analysis with application to geochronology and thermodynamics: *Geochimica et Cosmochimica Acta*, v. 51, p. 2129–2135, doi: 10.1016/0016-7037(87)90261-4.
- Roeske, S.M., Dusel-Bacon, C., Aleinikoff, J.N., Snee, L.W., and Lanphere, M.A., 1995, Metamorphic and structural history of continental crust at a Mesozoic collisional margin, the Ruby terrane, central Alaska: *Journal of Metamorphic Geology*, v. 13, no. 1, p. 25–40.
- Roeske, S.M., Till, A.B., Layer, P.W., and Harms, T.A., 2003, Kobuk fault zone of the southern Brooks Range, Alaska preserves Paleocene exhumation of amphibolite-grade rocks along a dextral-slip fault system: *Geological Society of America Abstracts with Programs*, v. 36, no. 5, p. 474.
- Saltus, R.W., Phillips, J.D., Till, A.B., Stanley, R.G., and Morin, R.L., 2004, Geophysical evidence that oceanic rocks underlie the Yukon Flats basin, Alaska: *Geological Society of America Abstracts with Programs*, v. 36, no. 5, p. 495.
- Samson, S.D., and Alexander, E.C., 1987, Calibration of the interlaboratory  $^{40}\text{Ar}/^{39}\text{Ar}$  dating standard, MMhb-1: *Chemical Geology*, v. 66, p. 27–34.
- Silberman, M.L., Moll, E.J., Chapman, R.M., Patton, W.W., Jr., and Connor, C.L., 1979, Potassium-argon age of granitic and volcanic rocks from the Ruby, Medfra, and adjacent quadrangles, west-central Alaska, in Johnson, K.M., and Williams, J.R., eds., *The United States Geological Survey in Alaska: Accomplishments during 1978: U.S. Geological Survey Circular 804-B*, p. B63–B68.
- Sisson, V.B., Pavlis, T.L., Roeske, S.M., and Thorkelson, D.J., 2003, Introduction: An overview of ridge-trench interactions in modern and ancient settings, in Sisson, V.B., Roeske, S.M., and Pavlis, T.L., eds., *Geology of a Transpressional Orogen Developed during Ridge-Trench Interaction along the North Pacific Margin: Geological Society of America Special Paper 371*, p. 293–326.
- Spear, F.S., and Cheney, J.T., 1989, A petrogenetic grid for pelitic schists in the system  $\text{SiO}_2\text{-Al}_2\text{O}_3\text{-FeO-MgO-K}_2\text{O-H}_2\text{O}$ : *Contributions to Mineralogy and Petrology*, v. 101, p. 149–164, doi: 10.1007/BF00375302.
- Stacey, J.S., and Kramers, J.D., 1975, Approximation of terrestrial lead isotope evolution by a two-stage model: *Earth and Planetary Science Letters*, v. 26, p. 207–221, doi: 10.1016/0012-821X(75)90088-6.
- Steiger, R.H., and Jaeger, E., 1977, Subcommittee on geochronology: Convention on the use of decay constants in geo and cosmochronology: *Earth and Planetary Science Letters*, v. 36, p. 359–362, doi: 10.1016/0012-821X(77)90060-7.
- Tempelman-Kluit, D.J., 1979, Transported cataclasite, ophiolite, and granodiorite in Yukon: Evidence of arc-continent collision: *Geological Survey of Canada Paper 79-14*, 27 p.
- Thirlwall, M.F., 2000, Inter-laboratory and other errors in Pb isotope analyses investigated using a  $^{207}\text{Pb}$ - $^{204}\text{Pb}$  double spike: *Chemical Geology*, v. 163, p. 299–322, doi: 10.1016/S0009-2541(99)00135-7.
- Till, A.B., and Snee, L.W., 1995,  $^{40}\text{Ar}/^{39}\text{Ar}$  evidence that formation of blueschists in continental crust was synchronous with foreland fold and thrust belt deformation, western Brooks Range, Alaska: *Journal of Metamorphic Geology*, v. 13, no. 1, p. 41–60.
- Till, A.B., O'Sullivan, P., Bradley, D., and Roeske, S., 2004, Apatite fission-track evidence for repeated Tertiary movement on the Tintina fault system, Alaska: *Geological Society of America Abstracts with Programs*, v. 36, no. 5, p. 512.
- Till, A.B., Stanley, R.G., O'Sullivan, P.B., Saltus, R.W., and Crews, J., 2005, Tectonic events leading to establishment of the Yukon Flats basin, Alaska: *Geological Society of America Abstracts with Programs*, v. 37, no. 4, p. 94.
- Trop, J.M., Ridgway, K.D., and Spell, T.L., 2003, Sedimentary record of transpressional tectonics and ridge subduction in the Tertiary Matanuska Valley—Talkeetna Mountains forearc basin, southern Alaska, in Sisson, V.B., Roeske, S., and Pavlis, T.L., eds., *Geology of a Transpressional Orogen Developed during Ridge-Trench Interaction along the North Pacific Margin: Geological Society of America Special Paper 371*, p. 89–118.
- Underwood, M.B., Howell, D.G., Johnsson, M.J., and Pawlewicz, M.J., 1996, Thermo-tectonic evolution of suspect terranes in the Kandik Region of east-central Alaska: *U.S. Geological Survey Bulletin 2142*, p. 81–110.
- Van Kooten, G.K., Watts, A.B., Coogan, J., Mount, V.S., Swenson, R.F., Daggett, P.H., Clough, J.G., Roberts, C.T., and Bergman, S.C., 1997, *Geologic Investigations of the Kandik area, Alaska and adjacent Yukon Territory*, Canada: Alaska Division of Geological and Geophysical Surveys Report of Investigations 96-6a, scale 1:125,000, 3 sheets.
- Weber, F.R., and Foster, H.L., 1982, Tertiary(?) conglomerate and Quaternary faulting in the Circle quadrangle, Alaska: *Geological Survey Circular*, v. 844, p. 58–60.
- York, D., Hall, C.M., Yanase, Y., Hanes, J.A., and Kenyon, W.J., 1981,  $^{40}\text{Ar}/^{39}\text{Ar}$  dating of terrestrial minerals with a continuous laser: *Geophysical Research Letters*, v. 8, p. 1136–1138.